

Kepler Input Catalog: Photometric Calibration and Stellar Classification

Timothy M. Brown

Las Cumbres Observatory Global Telescope, Goleta, CA 93117

tbrown@lcogt.net

David W. Latham

Harvard-Smithsonian Center for Astrophysics, Cambridge, MA 02138

latham@cfa.harvard.edu

Mark E. Everett

National Optical Astronomy Observatories, Tucson, AZ 85721

everett@noao.edu

Gilbert A. Esquerdo

Harvard-Smithsonian Center for Astrophysics, Cambridge, MA 02138

gesquerd@cfa.harvard.edu

Received _____; accepted _____

ABSTRACT

We describe the photometric calibration and stellar classification methods used by the Stellar Classification Project (SCP) to produce the *Kepler* Input Catalog (KIC). The KIC is a catalog containing photometric and physical data for sources in the *Kepler Mission* field of view; it is used by the mission to select optimal targets. Four of the visible-light (g, r, i, z) magnitudes used in the KIC are tied to SDSS magnitudes; the fifth ($D51$) is an AB magnitude calibrated to be consistent with Castelli & Kurucz (2004) (henceforth CK) model atmosphere fluxes. We derived atmospheric extinction corrections from hourly observations of secondary standard fields within the *Kepler* field of view. For these filters and extinction estimates, repeatability of absolute photometry for stars brighter than magnitude 15 is typically 2%. We estimated stellar parameters $\{T_{\text{eff}}, \log(g), \log(Z), E_{B-V}\}$ using Bayesian posterior probability maximization to match observed colors to CK stellar atmosphere models. We applied Bayesian priors describing the distribution of solar-neighborhood stars in the color-magnitude diagram (CMD), in $\log(Z)$, and in height above the galactic plane. Several comparisons with samples of stars classified by other means indicate that for $4500 \text{ K} \leq T_{\text{eff}} \leq 6500 \text{ K}$, our classifications are reliable within about $\pm 200 \text{ K}$ and 0.4 dex in $\log(g)$ for dwarfs, with somewhat larger $\log(g)$ uncertainties for giants. It is difficult to assess the reliability of our $\log(Z)$ estimates, but there is reason to suspect that it is poor, particularly at extreme T_{eff} . Comparisons between the CK models and observed colors are generally satisfactory with some exceptions, notably for stars cooler than 4500 K. Of great importance for the *Kepler Mission*, for $T_{\text{eff}} \leq 5400 \text{ K}$, comparison with asteroseismic results shows that the distinction between main-sequence stars and giants is reliable with about 98% confidence. Larger errors in $\log(g)$ occur for warmer stars, for which our filter

set provides inadequate gravity diagnostics. The KIC is available through the MAST data archive.

Subject headings: catalogs — methods: data analysis — surveys — techniques: photometric

1. Introduction

The *Kepler Mission* (Borucki et al. 2010) surveys some 1.6×10^5 stars in a field covering roughly 150 square degrees, watching for short-lived dips in brightness that may signal transiting planets. Of special interest to *Kepler* are transits by Earth-size planets, which, if they involve Sun-size stars, give relative depths of about 10^{-4} , near to the practical limit of precision accessible by *Kepler*. For a planet of given size, the transit depth scales inversely as the cross-sectional area of the parent star. For this reason, the detectability of Earth-size planets depends strongly on the typical stellar radius of the sample of stars that *Kepler* observes. The number of stars that *Kepler* can follow is limited by telemetry bandwidth, and is considerably smaller than the total number of stars in *Kepler*'s field of view (FOV) that allow useful photometric precision. Thus, from an early stage the *Kepler* team recognized the importance of characterizing the radii of stars in the *Kepler* FOV, to prevent large-radius stars (e.g. giants) from taking slots on the target list away from smaller stars with better planet-detection prospects. The project instituted the Stellar Classification Project (SCP) in response to this need. The SCP's goal was to provide, for all plausible target stars in the *Kepler* FOV, estimates of important stellar parameters. These were principally the radius R , effective temperature T_{eff} , and apparent magnitude K_p (ie, as seen by the *Kepler* photometer) but also, to the extent possible, the surface gravity parameter $\log(g)$ and the metallicity parameter $[Z] \equiv \log(Z/Z_{\odot})$.

Because of the sky area and large number of stars involved, we deemed spectroscopic classification to be impractical, and instead chose to use broadband photometry, augmented by intermediate-band photometry using our custom $D51$ filter, which is sensitive to surface gravity and to metallicity. The results of this photometric reconnaissance of the *Kepler* FOV were federated with other suitable catalogs, such as 2MASS (Skrutskie et al. 2006), USNO-B1.0 (Monet et al. 2003), Hipparcos (ESA 1997; Perryman et al. 1997), Tycho2

(Høg et al. 2000), and UCAC2 (Zacharias et al. 2004) to become the *Kepler* Input Catalog, or KIC. The aim of this paper is to describe how we carried out the photometric analysis and stellar classification for the KIC. Details of the observing routine and of the photometric reductions will be given elsewhere, but a brief summary follows.

We took all observations with the 1.2m reflector at the Fred Lawrence Whipple Observatory on Mt. Hopkins, AZ. During the course of the project, we used a succession of three CCD cameras: the *4-Shooter* (from the project’s first data in September 2003 = JD 2452895 until August 2004 = JD 2453233), the *MiniCam* until September 2005 = JD 2453626, and the *KeplerCam* thereafter. All of these cameras had thinned, back-illuminated 4K x 4K pixel formats covering fields roughly 22 arcmin square, but the details of their detectors, noise properties, sensitivity, and geometry varied from camera to camera. To cover the entire *Kepler* field with these cameras required 1600 pointings with minimal (roughly 10%) overlap between adjacent pointings. We began observations with 7 filters (nominal Sloan u, g, r, i, z , and two special-order intermediate-bandwidth filters we termed $D51$ and G_{red}). Both of the latter had bandpasses of about 15 nm. The $D51$ filter, which was modeled after the Dunlap Observatory $DD51$ filter, was centered at 510 nm, and the G_{red} filter at 432 nm. In practice, we soon learned that the u and G_{red} filters required excessive exposure times, so we took very few observations with these filters, and we will henceforth ignore them for the most part.

For the great majority of the observations, we cycled through all of the filters at one pointing before moving to the next pointing. Each filter sequence consisted of both long and short integrations in the filters g, r, i, z . For g and z , the long and short exposure times were 30s and 3s; for r and i they were 20s and 2s. Filter $D51$ got only a single long integration of 160s. We identified 2 pointings containing stars that we used as secondary photometric standards; we returned to one of these fields about once per hour, so as to have a fairly

dense time sampling of the atmospheric extinction. We selected these two fields so that they included the open clusters NGC 6811 and 6819; the centers of these fields lay at {RA, Dec} of {294.56, +46.58} and {295.28, +40.23} (decimal degrees), and they contained 455 and 1181 secondary standard stars, respectively. Our intention, which we almost realized, was to visit each pointing at least 3 times under conditions of good transparency, never returning twice to a given pointing (except the standards) on the same night.

We used a special-purpose pipeline to reduce the image data to catalogs of star positions and apparent magnitudes (uncorrected for atmospheric extinction). This pipeline made the usual corrections for bias and flat field, identified star-like objects, used DAOPHOT (Stetson 1987) to perform PSF-fitting photometry and computed aperture corrections based on isolated bright stars, and fit an astrometric model to the stellar positions. We fitted the stellar PSFs using the DAOPHOT “Penny1” function, which has a Gaussian core and Lorentzian wings. The pipeline returned a list of detected stars (and starlike objects such as radiation events), with positions, magnitudes, sky background estimates, and shape parameters for each. Also returned were error estimates and various parameters relating to the image as a whole, including the starting time, exposure time, and estimated seeing width. All of these data were saved in an ASCII file and passed to the software that is the subject of the current paper. Here we describe the methods used for photometric calibration, correction for atmospheric extinction, and for interpretation of the resulting absolute photometry in terms of the physical parameters of the prospective *Kepler* target stars.

2. Strategy

The processes and software described here represent an intermediate stage in the processing of SCP data for the KIC. The functions of the procedure described here were

fourfold. First, it ingested the raw photometric catalogs provided by the photometry pipeline into a group of databases that allowed convenient processing. Second, it estimated the atmospheric extinction suffered by each measurement, and corrected the instrumental stellar magnitudes to yield calibrated ones. Third, it combined the calibrated magnitudes with other information (e.g. stellar atmosphere models) to estimate the physical parameters of each observed star, including T_{eff} , $\log(g)$, $[Z]$, radius R , mass M , and interstellar reddening E_{B-V} . Last, it discarded those stars (and putative stars) for which estimates were deemed unreliable.

Data ingestion was a straightforward process, with its details determined almost entirely by the database structure that was defined at the outset. Correction for atmospheric extinction was also simple in concept, depending mostly on the model adopted for extinction, and on the criteria for estimating the parameters in that model. Many of the latter decisions were guided by the choices made for the SDSS (Fukugita et al. 1996; Smith et al. 2002), since our filter set was similar to theirs.

Stellar parameter estimation was the most difficult part of the project. The underlying problem is that, for the purposes of the *Kepler* project, the most interesting parameter is the stellar radius R , which is to say $\log(g)$. But the (mostly) broadband filters we used provide measurements that are almost entirely insensitive to this parameter. The intermediate-band *D51* filter provides some gravity sensitivity, while for M-type stars, the $J - K$ color (obtained from the 2MASS catalog, Skrutskie et al. (2006)) provides a gravity measure. Nevertheless, the photometric information that we could obtain on the timescale necessary for the project was barely sufficient for our needs. It therefore made sense to perform the parameter estimation in the context of astrophysical information external to our photometry. We did this by adopting various distributions known for stars in the Sun’s neighborhood as Bayesian priors, and taking as each star’s physical parameters the ones

that maximized the posterior probability of obtaining the observed magnitudes and colors. As amplified below, this method had several drawbacks, but it did use the available data to far greater advantage than do methods that ignore the prior constraints. Many of the methods described below are devoted to ways of quantifying the needed prior distributions.

Finally, filtering out bad data and formatting the result for the next stage in KIC assembly was also straightforward, consisting mostly of identifying spurious detections, failed fits, and so on. The criteria for passing results to the final KIC are described below.

3. Calibrated Photometry

The data received from the photometric pipeline consisted of one ASCII file for each image taken at the telescope. Each file contained a header and two data tables. The header contained information relating to the image as a whole: Julian date, telescope coordinates, filter, exposure time, as well as various quantities such as PSF width, derived in the course of the analysis. The first data table contained the stars' coordinates obtained from an astrometric fit, their instrumental magnitudes, the local sky brightness, and various error estimates and goodness-of-fit parameters. The second table contained the coordinates, J, H, and K magnitudes, and unique integer identifier for all of the stars in the 2MASS catalog (Skrutskie et al. 2006) that fell within the field covered by the image in question.

To allow simple comparisons with results from the SDSS, we wished to place our photometry as nearly as possible on the Sloan system. Unfortunately the *Kepler* field lies entirely at low galactic latitude, so at the time we started the project, there were no SDSS data available inside the *Kepler* field. (This is no longer true, though SDSS coverage of the *Kepler* field remains very incomplete, with only a few square degrees of overlap in DR7.) We therefore chose a set of 8 fields elsewhere in the sky, each with data available from

SDSS DR1 (Abazajian et al. 2003; Stoughton & Jester 2004), to serve as our photometric standards. Subsequent SDSS data releases, notably DR2, had improved photometry. These improvements applied mostly to galaxies, however. Changes in methods for fitting “model” magnitudes gave modest reductions in the scatter for stellar magnitudes, but left the mean zero points unchanged (Abazajian et al. 2004).

We chose the standard fields first to span a range of RA surrounding the *Kepler* field, and also so that each contained a fairly wide range of stellar colors (but even so, there were many fewer blue than red stars in the standard fields). There were 284 primary standard stars; ignoring 6 evident outliers (which varied from the mean $(g - r)$, $(r - i)$ color-color relation by more than 0.5 magnitude), they spanned the range $-0.4 \leq (g - r) \leq 1.4$, and $-0.2 \leq (i - z) \leq 0.4$ (although the great majority of them lay within $0.3 \leq (g - r) \leq 0.8$). We observed several standard fields each night for several months at the beginning of the project, and used their time-averaged, extinction-corrected magnitudes to fit transformation coefficients between our internal magnitudes and the SDSS system. Subsequent visits to the standard fields provided assurance that our photometry was consistent.

Because of their source, primary standards did not have observed magnitudes in the D51 filter. To define the instrumental magnitude scale in this filter, we set the D51 magnitude for these stars so as to force agreement with model $(g - D51)$ colors, given the stars’ observed (SDSS) $(g - r)$ colors. We computed the model magnitudes used for this purpose from the Basel models (Lejeune et al. 1997) with $[Z] = 0$ and $\log(g) = 4.0$, and from the estimated wavelength response for the 1.2m telescope 4-Shooter camera. (We did not use the CK models for this purpose because they were not available at the early stage of the project when we did this calibration.)

The supplementary material contains a table listing all 284 of the primary standard stars, along with their photometric indices and the stellar parameters that we inferred for

these stars using the methods described below. The first few lines of this compilation are displayed in Table 1.

Later in the project, it was desirable to build reference fields of secondary standard stars. The stars in these fields had their magnitudes defined by repeated calibration against the primary standards. Two of the pointings that we used for secondary standards were chosen within the *Kepler* field itself. In the normal observing sequence, the telescope returned to one of these pointings on an hourly basis, so that we could obtain reliable measures of extinction in the part of the sky that was of most interest. Other secondary standard fields were defined near objects (for example, the cluster M67) that we wished to use in the astrophysical calibration of the photometry.

After obtaining a few dozen nights of data with all of the secondary standard stars, some stars could be identified as unsuitable because they showed large temporal variability, or they were members of close binaries, or for similar reasons. We removed these from the list of secondary standard stars.

3.1. Estimating Atmospheric Extinction Parameters

The extinction model was based on that used for the SDSS standard star grid (Smith et al. 2002), although in practice we found several of the coefficients in this model to be difficult or impossible to measure on a nightly basis, and we therefore set them to constant (sometimes zero) values. We partitioned our photometric observations into time-contiguous units termed *blocks*, with a block being a unit of data that could be adequately described by a single set of extinction coefficients. Almost always, blocks corresponded to entire observing nights. Sometimes, however, changing weather conditions made it desirable to subdivide a night into multiple blocks.

For filter i and an instance j (within a block) of observing a particular star k , our extinction model represented the observed magnitude m_{ijk} as follows:

$$m_{ijk} = m_{0ik} + a_i + k_i(X_{kj} - X_0) + b_i(C_{ik} - C_{0i}) + c_i(C_{ik} - C_{0i})(X_{kj} - X_0) . \quad (1)$$

Here m_{0ik} is the true magnitude of star k in filter i , $X_{kj} - X_0$ is the difference between the airmass of star k at instance j and a standard airmass X_0 , C_{ik} is the color of star k defined using a particular pair of filters similar in wavelength to the filter i , and C_{0i} is the color of a 'typical' star using that same filter pair. The coefficients a_i , k_i , b_i , and c_i are parameters that may be chosen to give the best fit to the observations.

Note that by writing the extinction as above, the 'standard' magnitude of a star corresponds to what one measures when the star lies at airmass X_0 , not when it is outside the atmosphere. One advantage of this approach was to reduce the effect of errors in estimation of the extinction per unit airmass (the k_i). Also, this choice of airmass coordinate tends to reduce correlated errors between a_i and k_i . For this analysis, we took the standard airmass X_0 to be 1.215. We chose this value to coincide with the value 1.3 adopted by SDSS, with allowance for the higher altitude (hence lower air density) of the Sloan telescope relative to the 1.2m telescope at Mt. Hopkins.

Note further that the extinction model makes no explicit assumption about, or measurement of, the site's mean extinction as a function of wavelength. All information about this behavior is contained in the coefficients a_i and k_i . As will be shown below, these vary enough from night to night that they call into question the utility of the site's mean color-dependence of extinction.

In practice, we found that the observations of standard stars on a single night ordinarily did not suffice to give a reliable estimate of all of the coefficients in the extinction relation.

Indeed, we obtained best results by fitting for the coefficients a_i each night, using values averaged over an entire observing season for the coefficients k_i , and taking the coefficients b_i from theoretical calculations based on model stellar fluxes and the estimated wavelength responses of the various filters. We took the coefficients c_i to be uniformly zero. Figure 1 shows the time variation of the coefficients a_i for all but 2 of the 205 nights for which we have data. The zero points on this Figure have been arbitrarily shifted for plotting clarity. The zero points are arbitrary, but time variations of the a_i coefficients have physical interest. Significant jumps in the a_i coefficients occurred with the inauguration of new cameras (changing from 4-shooter to MiniCam about JD 2453233, and from MiniCam to KeplerCam about JD 2453626). There also are trends and seasonal variations visible in these data, notably a loss of about 20% sensitivity in the telescope/KeplerCam system since the time the KeplerCam was installed.

After estimating the a_i coefficients, we produced a second estimate of the extinction and the quality of the night’s data. For this purpose we used only selected stars observed at each reference pointing to estimate the a_i and k_i coefficients for each night. We chose stars so that exactly the same subset of stars in each reference pointing were always used in the fitting process for a single night. This minimized errors arising from errors in the assumed magnitudes of the reference stars. We thus obtained nightly estimates of the k_i coefficients as well as the a_i (although the k_i are well-determined on a little less than half of the nights). Figure 2 illustrates such a fit for one fairly typical night. Frequent returns to reference fields within the *Kepler* FOV allow accurate fits for k on photometric nights, and reveal the times and severity of time-varying extinction on the (more common) non-photometric nights. The bottom panel shows residuals around the fits plotted against the measured image Full Width at Half Maximum (FWHM), measured in arcsec. An important part of the photometric reduction process was to perform seeing-dependent corrections for the fraction of starlight falling outside the boundaries of the effective photometric aperture. On

most nights, this plot showed no clear trend of residuals vs FWHM, but on some (such as the one illustrated here), there is slight evidence for such a trend. This indicates occasional errors in the aperture-correction procedures, which must compromise the photometry at some level. This problem was sporadic and relatively minor, making it difficult to diagnose. Indeed, we never succeeded in tracking this problem to its root, though plots such as those in Figure 2 allowed us to identify problematic nights. Also evident from this plot is the relatively large FWHM of the images on the night displayed here. Indeed, the images were broad on a large fraction of our observing nights; the image FWHM was below 1.7 arcsec only about 2% of the time, and the median FWHM for all of our images was 2.5 arcsec. Because of this relatively poor spatial resolution, the KIC is ineffective at distinguishing the components of binary stars, if their component separation is even moderately small.

Figure 3 shows the variation of the k_i with time, measured on the nights when we judged the observations to be consistent enough to allow a measurement. The night-to-night variations tend to be large (up to 40% of the mean values), but they are also well-correlated among filters. Thus, there is good evidence for variations dominated by large-particle aerosol extinction, having little wavelength dependence, and varying on a time scale of one to a few days. The SCP photometry could be improved by putting this information about the k_i back into the extinction model on a nightly basis. We have not yet done this, however. The corrections would not be large, in any case. Given the size of the errors in k and the typical difference between the airmasses of actual observations and the standard airmass ($X_0 = 1.215$), corrections in the observed magnitudes would be at most 0.09 mag, and would be less than .03 mag for about 90% of the observations.

After estimating the extinction coefficients for a block of data, we estimated the m_{i0} magnitudes averaged over visits for every star that was observed in any filter within that block. This process identified every star that was observed at any time during a given

block, and then gathered together every observation to be found in the databases for each of those stars.

Of the 1600 pointings that span the entire *Kepler* field, none have zero visits with acceptable photometry, 8% were visited only once, 71% twice, 17% three times, and 3% four or more times. Two pointings, corresponding to secondary standard fields, were visited more than 260 times each. For pointings with at least 4 visits, we computed a pseudo-*RMS* from the interquartile dispersion q as $RMS = q/1.349$; this formula gives the expected result for a gaussian distribution, but is insensitive to a small proportion of extreme outliers. we identified outliers as measurements differing from the median by more than 5 times this pseudo-*RMS*, and discarded them from the fit to give robust minimum- χ^2 magnitude estimates.

3.2. Precision of Corrected Magnitudes

We assessed the precision (in the sense of repeatability) of stellar magnitude estimates by collecting all the measurements for each star in the secondary standard fields (each having typically hundreds of individual observations), and computing the scatter in these time series. We did this for a set of 5652 stars brighter than $r = 19.5$, each having at least 50 individual observations (and most having more than 200). For each star we estimated the time-series pseudo-*RMS* as described above. We then computed for each filter the median pseudo-*RMS* taken over stars, in 1-magnitude bins centered on integral values of the (time-series) median magnitude. The resulting pseudo-*RMS* scatter as a function of stellar magnitude in each filter is plotted in Figure 4. The photometric errors are dominated by brightness-independent processes (probably errors in the atmospheric extinction correction) in all filters for stars brighter than about magnitude 14; for fainter magnitudes, photon statistics begin to have an effect, and become dominant by about magnitude 16. For the

stars brighter than magnitude 14, the repeatability of extinction-corrected measurements is about 2%, almost independent of filter.

The RMS precision of color estimates (ie, differences between magnitudes measured in different filters) was usually somewhat better than for magnitudes (typically 1.5%), because much of the scatter in the extinction-corrected magnitudes comes from extinction processes that have long time scales, whereas the two measurements making up a color estimate were almost always taken within a few minutes of each other.

4. *Kepler* Magnitudes

To estimate planet detectability for each potential target star, the *Kepler Mission* required information about stellar magnitudes as they would be measured by the *Kepler* photometer. These are known as the *Kepler* Magnitudes, or K_p . For this purpose we estimated *Kepler* Magnitudes using photometry in standard bandpasses. The K_p values that we computed for each star are tabulated in the KIC along with the other photometry. The ideal *Kepler* wavelength response function $K_I(\lambda)$ may be found in Koch et al. (2010) and on the *Kepler* web site ¹. The bandpass may be roughly described as having sharp edges, with the center being slightly peaked; it has more than 10% response in the wavelength range $420 \leq \lambda \leq 890$ nm. Thus, the bandwidth is about 470 nm and the effective wavelength, for an SED corresponding to a 5500 K black body, is approximately 665 nm.

The K_p are defined as *AB* magnitudes (Oke 1974; Smith et al. 2002), derived from each target’s calibrated g, r, i magnitudes. To compute them, we started with the published (Castelli & Kurucz 2004) grid of stellar atmosphere model fluxes, and used these and the

¹<http://keplergo.arc.nasa.gov/CalibrationResponse.shtml>

known, tabulated wavelength response functions to compute the rate of photoelectron detections from each of the model flux distributions for a wide range of stellar types (these were functions of T_{eff} , $\log(g)$, and metallicity) using each of the filters $\{g, r, i\}$ and using the “ideal” *Kepler* bandpass K_I described above. We then attempted to approximate these synthetic magnitudes as they would be measured in the band K_I in terms of linear combinations of the $\{g, r, i\}$ magnitudes for the corresponding models. Based on a visual inspection of the relationships, we defined these combinations on each of several contiguous ranges of some fiducial color, e.g. $(g - r)$; for operational purposes, K_p is defined only in terms of these combinations of magnitudes in standard filters.

Complications arise because not all KIC stars have valid values for all of the filters $\{g, r, i\}$, and moreover many stars (which appear in the KIC by virtue of federation with non-SCP catalogs) have none of them. The *Kepler* Magnitude K_p is thus defined by a complex set of rules, depending on what information is available about the star in question. Policy demanded that the KIC contain a Kepler magnitude for every star known to lie within the field. Thus, the rules covered cases in which information was scant and accurate transformations were not possible.

We note that the definition of K_p as a linear combination of observed magnitudes in standard bands means that the effective wavelength response function that one should ascribe to K_p is ill-defined. Apart from the ambiguity arising from which bands may have been used in computing K_p , it develops that (because of the nonlinear relation between flux and magnitude) the effective bandpass for K_p is also a function of the stellar color. Thus, the magnitudes K_p are entirely defined by the following Equations (2 through 6). A further result of the method for computing K_p is that the photometric zero point for K_p is not exactly on the AB system but is rather a weak function of stellar color. Because we chose the weighting coefficients for the various bandpasses based on a color-dependent fit

to integrals over $K_I(\lambda)$, the part of the zero point dependence that is linear in color has been absorbed by the weighting coefficients. Higher-order terms remain, however. At worst, for stellar colors at the extreme ends of the ranges that one encounters, these higher-order terms amount to about 0.05 mag.

For stars with SCP photometry, the computation rules are as follows.

If only one of $\{g, r, i\}$ is valid, then K_p is equal to the valid magnitude.

If only g and r are valid, then

$$K_p = 0.1g + 0.9r, \quad (g - r) \leq 0.8, \quad (2a)$$

$$K_p = 0.2g + 0.8r, \quad (g - r) > 0.8. \quad (2b)$$

If only g and i are valid, then

$$K_p = 0.55g + 0.45i, \quad (g - i) \leq -0.05, \quad (3a)$$

$$K_p = 0.3g + 0.7i, \quad (g - i) > -0.05. \quad (3b)$$

If only r and i are valid, then

$$K_p = 0.65r + 0.35i, \quad (r - i) \leq 0.673, \quad (4a)$$

$$K_p = 1.2r - 0.2i, \quad (r - i) > 0.673. \quad (4b)$$

If $\{g, r, i\}$ are all valid, then

$$K_p = 0.25g + 0.75r, \quad (g - r) \leq 0.3, \quad (5a)$$

$$K_p = 0.3g + 0.7i, \quad (g - r) > 0.3. \quad (5b)$$

The linear combinations in Eqns. (3), (4), and (5) yield K_p magnitudes that reproduce the “ideal” magnitudes K_I with typical errors of about 0.03 mag for stars with $T_{\text{eff}} \geq 3500\text{K}$,

though for extreme stellar parameter values, the errors may reach ± 0.2 mag. In the case in which only g and r are known (Eqns. 2), the disagreement between K_p and K_I may reach 0.6 mag for very cool M-type stars, in the sense that the computed K_p is fainter than K_I .

For stars imported from the Tycho-2 parent catalog, which gives B_T and V_T magnitudes, we estimate equivalent Sloan magnitudes g_T and r_T as

$$g_T = 0.54B_T + 0.46V_T - 0.07, \quad (6a)$$

$$r_T = -0.44B_T + 1.44V_T + 0.12, \quad (6b)$$

and then compute K_p using Eqns. (2a), (2b).

For stars coming from any other parent catalog having a both blue and a red magnitude, we simply substituted these magnitudes for g and r respectively, and again used Eqns. (2a), (2b).

Finally, for stars coming from parent catalogs that contain information in only one optical bandpass, K_p is taken to be the reported magnitude in that bandpass. In this case, of course, very large errors (1 mag or more) may occur.

5. Model Stellar Atmospheres

The stellar classification process requires choosing among model stellar atmospheres (which have parameters $\{T_{\text{eff}}, \log(g), \log(Z)\}$) so as to best fit the photometric observations. We used model atmospheres by Castelli & Kurucz (2004); these cover $3500K \leq T_{\text{eff}} \leq 50000K$, $0 \leq \log(g) \leq 5.5$, and $-3.5 \leq \log(Z) \leq 0.5$, although not all gravities are represented at all temperatures.

The models provide fluxes as a function of wavelength. To convert these to stellar AB magnitudes (relative to an arbitrary zero point) we transformed the tabulated values

from units of energy flux per unit wavelength to units of photon flux per unit frequency, multiplied the stellar flux by an estimate of the CCD response and by the estimated filter transmission functions, and integrated the result over frequency. to give the rate of photoelectron production as a function of filter and of each of the parameters that characterize the model atmospheres. We took magnitudes in each of the filters to be on the AB magnitude scale. In operational terms this was already the case for the filters $\{g, r, i, z\}$ and for the 2MASS magnitudes $\{J, H, K\}$; we therefore left the zero points in all of these filters untouched. For the D51 filter, we adjusted the zero point to force agreement with the CK model $g - D51$ colors as described in section 3.

After computing the stellar magnitudes described above, we next formed differences to yield 7 independent colors, viz., $(g - r), (r - i), (i - z), (z - J), (J - H), (H - K), (g - D51)$. The arbitrary zero point cancels from these differences, so these numbers are a representation of the spectral energy distribution of the stellar models that does not depend upon stellar radii or distances. Most of the operations that later tried to match stellar properties to observations relied on these 7 colors.

To achieve near equality between observed colors and fluxes from the CK models, we transformed the latter in several ways. First, we adjusted the magnitude zero points for all filters except i (which we adopted as standard, linked by definition to a small set of SDSS stars). We based these adjustments on comparisons with 3 sets of stars for which the photometric (and in some cases the physical) properties could be known with some accuracy from pre-existing data. These included a set of 4 Sun-like stars chosen from the list of SDSS standard stars (Smith et al. 2002), a set of 63 to 77 stars (depending on the filter involved) in the cluster M67, each of them known to be single from spectroscopic observations by W. Latham and S. Meibom, and having good photometry and spectroscopic classification (Montgomery et al. 1993; Sandquist 2004), and finally a set of some 500 probable cluster

stars in a 2-degree square surrounding M67. For the last group, we first identified an optimally-fitting stellar atmosphere model for each star that fell close to the M67 cluster isochrone, and then adjusted the magnitude zero points to minimize the mean difference between observed and predicted colors.

Second, we noted a serious disagreement between observed and model $(g - r)$ colors for stars cooler than 4000 K. Model $(g - r)$ colors based on the CK fluxes never exceed about 1.2, while many faint members of M67 and nearby field stars (which are almost certainly dwarfs of near-solar metallicity) have $(g - r)$ colors that approach 1.5. To allow more accurate modeling of the photometry for these stars, we applied ad hoc adjustments to the $(g - r)$ colors of all CK models with temperatures of 4000K or less. These adjustments added to each model $(g - r)$ value an offset that depended only upon T_{eff} . The corrections applied were +0.179 at 4000K, +0.289 at 3750K, and +0.402 at 3500 K. This ad hoc process improved the quality of fits considerably, but rendered the T_{eff} scale in this range unphysical, at least so far as the $(g - r)$ color is concerned.

Third, we added smaller T_{eff} -dependent corrections to the colors $\{(r - i), (i - z), (J - H), (H - K)\}$. These corrections were linear in temperature and equal to zero at $T_{\text{eff}} = 5000\text{K}$, with slopes per 1000K equal to $\{.006, -.021, -.036, .011\}$ respectively, . All of these adjustments were independent of $\log(g)$ and $\log(Z)$.

Last, we adjusted the $(g\text{-D51})$ color in a way that depended both on T_{eff} and on $\log(g)$: for $T_{\text{eff}} \leq 4300\text{K}$, the revised model color $(g - D51)'$ was given by

$$(g - D51)' = (g - D51) - 0.23f_g(T_{\text{eff}} - 4300)/1000. \quad (7)$$

where the function $f_g(\log(g))$ was unity for $\log(g) \geq 3.5$, and for smaller $\log(g)$ decreased linearly with $\log(g)$ to zero at $\log(g) = 0$.

6. Reddening

Interstellar reddening is significant for most of the stars in the *Kepler* field, so it was necessary to include it in the models of stellar colors. We assumed that the wavelength dependence of reddening is described by the formalism of Cardelli et al. (1989). In all cases we used $R_V = 3.1$, which Cardelli et al. found to be the typical value for diffuse interstellar dust clouds.

Strictly, the reddening suffered by starlight depends on the spectrum of the star, and hence on its parameters $\{T_{\text{eff}}, \log(g), \log(Z)\}$. The importance of this effect is fairly small, however, so for speed of computation, we precomputed reddenings for our filters and a range of stellar parameters. We then adopted the reddening vectors for typical stars in the *Kepler* field ($T_{\text{eff}} = 5000\text{K}$, $\log(g) = 4.0$, $\log(Z) = 0$) as applying to all stars.

We estimated the strength of the reddening using a simple model of the dust distribution in the Milky Way. This model assumed that dust is distributed in a smooth disk aligned with the plane of the Milky Way, having an exponential decay of density with height above the plane. For all computations described here (except for certain test cases, such as parameter estimations for M67), we took the e-folding height for disk density to be 150 pc, which is slightly larger than suggested by recent estimates (Koppen & Vergely (1998); Marshall et al. (2006) give 140 pc, 125 pc, respectively). We took the density in the plane to be such as to cause 1 magnitude of extinction in the V band in a path length of 1000 pc (Koppen & Vergely 1998).

7. Fitting Stars to Observations: Linked Parameters

A star and the light we see from it may be characterized by many parameters, not all of them independent. These include not only its photometric colors, but also its apparent

magnitude, distance, reddening, and intrinsic properties $\{T_{\text{eff}}, \log(g), \log(Z)\}$, mass M , radius R , and luminosity L . Different photometric measurements constrain different combinations of these parameters; to obtain sensible estimates of the intrinsic parameters, it is important to respect the relations that connect them.

We took our distinct observables to be the photometric colors (in the typical case for which u and G_{red} are unavailable, there are 7 of these), the apparent magnitude in any one filter (we used r), and the galactic latitude b . The eleven parameters we wished to estimate were $T_{\text{eff}}, \log(g), \log(Z), M, R, L, BC_r, d, A_r, A_V, E_{B-V}$, where BC_r is the bolometric correction for the r band (in practice computed as $BC_r = BC_V + (V - r)$), d is the distance in pc, A_r and A_V are the interstellar extinction in the r and V bands, and E_{B-V} is the $B - V$ color excess due to interstellar extinction. But connecting these parameters are the relations:

$$A_r = \kappa_r \int_0^d \exp(-s \sin b) ds \quad (8)$$

$$A_V = A_r/0.88 \quad (9)$$

$$E_{B-V} = A_V/3.1 \quad (10)$$

$$L = R^2(T_{\text{eff}}/T_{\odot})^4 \quad (11)$$

$$r = r_{\odot} - 2.5 \log L + BC_r + A_r + 5 \log d - 5 \quad (12)$$

$$\log(g) = \log(g)_{\odot} + \log M - 2 \log R \quad (13)$$

where κ_r is the assumed r -band interstellar extinction coefficient in magnitudes per pc, R , M , and L are in solar units, d and the dummy integration variable s are in pc, r_{\odot} is the Sun's absolute magnitude in the r band, and A_r , A_V , BC_r , and E_{B-V} are in magnitudes. The simple numerical relations between A_r , A_V , and E_{B-V} result from integrating the Cardelli et al. model of interstellar reddening against typical (5000K dwarf) stellar flux distributions, as described above.

Applying the above constraints reduced the number of unknowns from 11 to 5, but this was still an uncomfortably high-dimensional space to search for best goodness-of-fit. Worse, given realistic errors in the data, we found that an unrestricted search in this space tended to lead to unphysical solutions in which various parameters were driven to extreme values in an attempt to balance misfits relative to the observations. To reduce these problems we adopted two further ad hoc relations, namely

$$BC_r = BC_r(T_{\text{eff}}, \log(g)) \quad (14)$$

and

$$M = M(T_{\text{eff}}, \log(g)) \quad (15)$$

The BC_r relation is valid for fixed composition, and for computational purposes we simply adopted the results of the CK models for $\log(Z) = 0$. We justify the inaccuracies resulting from ignoring the $\log(Z)$ dependence by the relative scarcity of low-metallicity stars in the solar neighborhood.

The $M(T_{\text{eff}}, \log(g))$ relationship is true only in a statistical sense, because age and (to a lesser extent) metallicity effects cause the evolutionary tracks of stars of different mass to cross in the CMD. This causes inevitable ambiguity, especially for giants and subgiants. However, for the cool main-sequence stars that are of the most interest to *Kepler*, the approximation is fairly good. To estimate this relation, we took stellar evolution isochrones by Girardi et al. (2000), and weighted each by its age (thus, in effect, assuming a constant star formation rate), with 5 isochrones covering ages between 63 My and 4.5 GY. We then smoothed the resulting distribution of masses in $\log(T_{\text{eff}}) - \log(g)$ space to yield typical masses at each point.

Having adopted the $BC_r(T_{\text{eff}}, \log(g))$ and $M(T_{\text{eff}}, \log(g))$ relationships, we saw that at the same level of consistency, several other useful parameters of stars could also be treated as being functions only of T_{eff} and $\log(g)$. These included the luminosity L , the $V - r$

color (used in relating extinction to distance), and absolute magnitudes in V and r bands. Thus, we precomputed tables for all of these quantities, and interpolated into the tables as necessary to give values for any of these quantities as functions of T_{eff} and $\log(g)$.

The process of computing a goodness-of-fit statistic for an individual star then proceeded as follows. We first fetched the observed colors, the r magnitude, and the galactic latitude b for each star. We then performed a straightforward (ie, not particularly efficient) search in $\{T_{\text{eff}}, \log(g), \log(Z)\}$, seeking the minimum value of a merit function that is the sum of a χ^2 statistic based on the photometry and the negative logarithm of a prior probability. This section describes the χ^2 computation; the justification for this general Bayesian procedure and the computation of the prior probability distribution will be described below. The search for the minimum involved evaluating the merit function on successive 2-dimensional subsets of the search space; for practical purposes this meant evaluating model colors for a grid of models, each with specified T_{eff} , $\log(g)$, and $\log(Z)$, and each relating to a star with a specified r magnitude and galactic latitude. We did this by using an interpolated table look-up to give L , BC_r , and $V - r$ from T_{eff} and $\log(g)$, and then computing the distance d and extinction from r , b , and the galactic extinction model. We then generated model colors for each T_{eff} , $\log(g)$, $\log(Z)$ in the current grid of interest, and, knowing the extinction for each of these, applied a corresponding reddening correction to the model colors. Last, we differenced the observed and model colors, and (using the estimated observational errors) computed a χ^2 value for each grid point.

For some stars, not all of the $g, r, i, z, D51$ data were available. In these cases, we set the uncertainty for the missing data to 10^5 magnitudes, assuring that the actual values made no contribution to the fit.

8. Bayesian Posterior Probability Estimation

When fitting stellar parameters to our photometric data, we found that pure χ^2 minimization often led to unreasonable results. This is because outlandish combinations of the stellar parameters, corresponding to stars that are seldom or never seen in nature, may yield marginally better fits to the observations than do more plausible parameter combinations.

Bayesian methods provide a way to control this behavior. To describe the application of Bayes' Theorem to the stellar classification problem, we denote the intrinsic stellar parameters $\{T_{\text{eff}}, \log(g), \log(Z)\}$ by the vector \mathbf{x} , and the various photometric observations of a particular star by the vector \mathbf{q} . We assume that we know something about the statistical distribution of stars, so that it is meaningful to talk about the prior probability distribution $P_0(\mathbf{x})$, where the probability that a given star lies within a small volume of parameter space is given by $P_0(\mathbf{x})d\mathbf{x}$. Then Bayes' Theorem says that if we add to this a priori information about stars a set of observations \mathbf{q} relating to a particular star, then the updated (posterior) probabilities are

$$P(\mathbf{x}|\mathbf{q}) = [P_0(\mathbf{x})P(\mathbf{q}|\mathbf{x})]/P_0(\mathbf{q}) \quad . \quad (16)$$

The choice of stellar parameters that maximizes the posterior probability is then the choice of \mathbf{x} that maximizes this expression. Here the denominator, the a priori probability of observing photometric indices given by \mathbf{q} , is a normalization that does not depend upon the parameters \mathbf{x} of interest; for purposes of maximizing the posterior probability, it may be ignored. In the ideal case of independent Gaussian errors in the photometric observations, one can write

$$P(\mathbf{q}|\mathbf{x}) = \exp(-\chi^2/2) \quad , \quad (17)$$

where χ^2 (not the reduced χ^2) is the usual goodness-of-fit statistic. Taking the logarithm of the posterior probability, it follows that maximizing this probability is equivalent to

maximizing

$$\ln P(\mathbf{x}|\mathbf{q}) = \ln P_0(\mathbf{x}) - \chi^2/2 . \quad (18)$$

This is what the stellar parameter-estimation procedures try to do.

It is well known that Bayesian methods have both advantages and disadvantages. In the current case one advantage is that wildly implausible stellar classifications are ruled out a priori; the emerging values of $\{T_{\text{eff}}, \log(g), \log(Z)\}$ are guaranteed to resemble those of known kinds of stars. The corresponding disadvantage is that stars with rare properties are almost certain to be misclassified, since such stars are represented insignificantly or not at all in the statistical samples that one uses to estimate $P_0(\mathbf{x})$. The Bayesian maximization places stars in the most plausible of the already-existing pigeonholes; if the data are poor or contradict expectations for known kinds of objects, incorrect classifications may occur.

Thus, for the principal *Kepler* purpose of distinguishing GKM-type dwarfs from giants, the Bayesian approach can be expected to work well. For other purposes (identifying possible brown dwarfs, say, or distant highly-reddened blue supergiants), it is better to rely directly on the photometry, and ignore the classifications.

Another problem with Bayesian estimation is that commonly there is no good basis for estimating prior probabilities. Fortunately, in the case of stellar classification, one can do rather well. For purposes of the KIC classification, we expressed $P_0(\mathbf{x})$ as the product of 3 terms:

$$P_0(\mathbf{x}) = P_{CMD}[T_{\text{eff}}, \log(g)]P_Z[\log(Z)]P_z(z) , \quad (19)$$

where P_{CMD} describes the probability density of stars in the $T_{\text{eff}} - \log(g)$ plane, and P_z gives the probability density with height above the galactic plane z . Expressing P_0 as a product distribution implicitly assumes that there are no correlations among the various dependencies. Of course, this is not completely true. Because of the relations between age and Z , and between age and z , the product distribution is not strictly valid. The

relatively low frequency of old, low-metallicity stars makes this distribution a reasonable approximation, however. Nevertheless, as we have implemented it, the classification scheme knows nothing of (say) the existence of old low-metallicity halo stars, nor of the absence of young low-metallicity stars, etc.

To estimate P_{CMD} , we used the Hipparcos (ESA (1997); Høg et al. (2000)) catalog to create a histogram of the nearby star distribution, sampled in $(B - V)_{Tycho}, V_{abs}$ space. For this purpose we took all the Hipparcos stars with parallaxes that are known to better than 10%. This sample contained 9590 stars. We then mapped the $B - V$ color and absolute V magnitude into $\log(T_{\text{eff}})$ and $\log(g)$. Once each star was associated with its calculated T_{eff} and $\log(g)$, it was a simple matter to construct a histogram giving the fraction of stars found within each cell in that space.

After creating the histogram of star frequencies in $T_{\text{eff}} - \log(g)$ space, we performed several edits and additions to make it more realistic, complete, and useful. We first set star frequencies to zero for regions where only 1 or 2 stars were found in isolated cells. We next added stars to the area of the histogram occupied by bright giants, since the volume covered with good parallax precision by Hipparcos is not large enough to populate this part of the diagram. We then scaled the frequencies for intrinsically faint stars to account for the search volume that is implied by the stellar absolute magnitudes, since this volume is determined by the astrometric precision only for relatively bright stars. After doing this, the very faintest M stars were still unrepresented, so we added stars to populate the faint tail of the main sequence. Finally, we smoothed the histogram to yield one that represents the broad features of the local stellar population, but that has little small-scale structure. We took the natural logarithm of this histogram to be the logarithm of P_{CMD} .

To estimate $P(Z)$, we used the compilation by Nordström et al. (2004) of metallicities for about 14000 bright nearby stars. We first used these data to construct a histogram of

$\log(\text{relative frequency})$ at equally-spaced intervals in $\log(Z)$. We then fit a polynomial to these histogram values, and made a linear extrapolation of the polynomial for $\log(Z) \leq -3$ and for $\log(Z) \geq +0.9$. We then evaluated this extrapolated polynomial to compute our estimate of $P(\log(Z))$.

For the distribution of stars as a function of the height z above the galactic plane, we assumed the galactic disk’s number density to decrease exponentially with a vertical scale height of 300 pc (Cox (2000) p. 482). In the probability distribution, we also allowed for the cubic increase in sample volume (per unit solid angle and apparent stellar magnitude) with increasing distance.

With these probabilities in hand, we were able to compute the natural logarithm of the prior likelihood $\ln(P_0(\mathbf{x}))$, according to Eqn. (19).

9. Star Selection, Formatting, and Output

When constructed as just described, the KIC contained a large fraction of spurious objects. These were mostly photometric artifacts that appeared only once in all of our (multi-filter, multi-visit) catalogs. The causes for these included near-threshold noise detections, radiation events, diffraction artifacts near bright stars, ghost images caused by crosstalk among the CCD quadrants, residual cosmetic defects in the CCDs, and perhaps other sources that we have been unable to identify. To remove such invalid data from the KIC, we discarded all supposed stars that did not have at least 2 valid optical measurements or 3 NIR measurements. This rejection step removed a large fraction (about 2/3) of the entries from the star catalog. Although this fraction appears very large, one must recall that each pointing accumulated spurious detections (eg, radiation events) from images taken with every filter and at every visit, whereas the inventory of real stars remained

nearly constant. Thus, the secondary standard pointings, which we visited hundreds of times each, were prolific sources of false entries in the initial catalog of detected objects.

Next, we set the astrophysical parameters $\{\log(g), \log(Z), A_V, E_{B-V}\}$ to be “invalid” for all stars where the number of valid measurements in visible-light filters was less than 4, or where the stellar parameter estimation code did not converge. This step typically caused only a small fraction of the remaining stars to be assigned “invalid” physical parameters. We set the parameter T_{eff} to “invalid” only if there was no valid optical color, which is to say, 2 or fewer valid visible-light magnitudes.

For a description of all of the data fields contained in the KIC, see the “Kepler FOV Field Descriptions” page on the MAST/KIC web site.²

10. Photometric Diagnostics and Validation of Stellar Classifications

The stellar parameters we assigned to stars were, by construction, distributed in the CMD diagram in plausible ways, and did not conflict with schematic constraints about the spatial and metallicity distribution of stars in the galaxy. But of course these statistical properties of the KIC do not guarantee that individual stars are correctly classified, even though correct classification of individual stars is precisely what the catalog must provide, to serve its purpose. The classifications can fail at many stages in the process. It is hopeless to expect good classifications out of bad photometry, but on many nights the atmospheric conditions were imperfect, or there were problems with the telescope or other instrumentation. Thus, we needed diagnostics of the quality of the photometry, with as much time resolution as we could manage. Also even good photometry can yield poor classifications if there are systematic errors in the models to which the photometry is

²http://archive.stsci.edu/search_fields.php?mission=kepler_fov

compared, or if there are true degeneracies in the model-fitting, or if the mathematical model-fitting problem is ill-posed and unduly sensitive to noise. For these reasons it was important to test the classification procedures by comparing their results with independent estimates of the same stellar parameters, obtained from different data sets. There proved to be a number of ways to make such comparisons for restricted sets of stars, and such comparisons have become easier as ground-based observations have been concentrated on the *Kepler* field, and as *Kepler* itself has returned variability information about many target stars. The degree to which the KIC can be validated nevertheless remains rather unsatisfactory; future studies will doubtless give more complete pictures of the successes and failures of the classification scheme. In the following sections, we describe the diagnostics that we used as quality control measures while compiling the KIC, and a few of the validation tests that we have performed.

10.1. Quality of fits to the photometry

A simple test of the parameter-fitting process is to compare observed colors for each star with those predicted for the derived stellar parameters $\{T_{\text{eff}}, \log(g), \log(Z), E_{B-V}\}$. We made plots showing this comparison for each 1-degree-square tile in the *Kepler* field. Within each such tile, we selected stars for which the fit for stellar properties converged, and for which all of the magnitudes $\{g, r, i, z, D51, J, H, K\}$ had valid values. For each star in this set, we computed model colors. We then formed the difference between the observed colors and the model ones. Each panel of Figure 5 shows the differences plotted as points on a different color-color diagram (eg $(r - i)$ vs $(g - r)$, or $(J - K)$ vs $(g - i)$). The colors were chosen so that every filter is represented at least once. Of interest are the centroids of the plotted clouds of points, their scatter in each color, and the presence or absence of correlations between the residuals in different colors.

For the most part, the fitting process appears to have worked well: for tiles at relatively high galactic latitude (7 degrees and above), the residuals have nearly zero mean in all colors, with distributions that are more or less Gaussian. Some colors have more scatter than others – this is the case for any color involving a 2MASS filter or Sloan z ; evidently the magnitudes in these filters are noisier than in the visible-light filters $\{g, r, i\}$ by a factor of about 2. Also, there are clear anticorrelations between several pairs of colors. Notably, $(r - i)$ and $(i - z)$ are anti-correlated, as are $(i - z)$ and $(z - J)$, and also $(J - H)$ and $(H - K)$. These correlations suggest excess scatter in the common filter of each of $(i, z, \text{ and } H)$. Analysis shows that these anticorrelations arise from two separate processes, one of which affects exclusively the 2MASS magnitudes, while the other is exclusively connected with the visible-light data. Beyond this, the causes of these effects are not yet clear. Tiles at very low galactic latitudes (less than 7 degrees) typically show much larger scatter than higher-latitude tiles, and also significant displacement of the mean residuals from zero. We suppose that these effects arise from large and spatially nonuniform interstellar extinction, but as yet we cannot rule out alternative explanations. About 3.3% of the area of the *Kepler* field of view lies at galactic latitudes of 7 degrees or less.

10.2. Giant-dwarf separation in color-color space

From the perspective of the *Kepler* mission, the most important task of the KIC is to correctly distinguish giant stars from dwarfs across the greatest possible range of T_{eff} . Figure 6 illustrates the photometric basis for the KIC’s classifications. Panel (a) shows the $(g - D51)$ vs $(g - r)$ color-color diagram for one tile covering one square degree of sky near $b = 10.5^\circ$. In both panels of Figure 6, stars classified as giants (defined as having $\log(g) < 3.6$) are indicated by heavy red symbols, and dwarfs (with larger $\log(g)$) are plotted as small black symbols. In Figure 6a, main-sequence stars occupy a locus that trends from

lower left to upper right as T_{eff} falls, until $(g - r) \approx 0.65$ is reached. At this point the $(g - D51)$ colors for dwarfs turn sharply blueward as $(g - r)$ continues to get redder. At $(g - r) \approx 1.0$ this trend reverses and the $(g - D51)$ color reddens rapidly. The result is that main-sequence stars form a sickle shape: hot stars form the handle of the sickle, and cooler ones form the (curved, concave upwards) blade. The area inside the blade of the sickle (and particularly the redward extension of the handle) is occupied by stars with lower surface gravity, or with low metallicity. In these stars the Mg b lines are weak compared to what one sees on the main sequence, resulting in more flux in the $D51$ band, and a more positive $(g - D51)$ color. Most often, plots like these show a clear demarcation between the dwarf- and giant-star regions, with few stars having contrary classifications appearing in either region.

Figure 6b shows $(J - K)$ plotted against $(g - i)$. As is well known (eg Bessell & Brett (1988)), color-color diagrams involving $(J - K)$ bifurcate for M-type stars, with main-sequence stars limited to $(J - K)$ colors smaller than about 0.9, while low-gravity (and also low metallicity) stars continue to grow redder with lower T_{eff} . Again, most plots show a clean separation between dwarfs and giants on this diagram, for $(g - i)$ colors that are red enough. Note that both panels of the Figure use dereddened colors, where the reddening $E_{B-V} = A_V/3.1$ is computed from the star’s galactic latitude and estimated distance, as described in Section 7.

10.3. Comparison of stellar parameters with stars in M67

Another useful test of the analysis procedure is to compare fitted parameters for a group of stars with those that can be reliably estimated using other means. One group of stars for which this comparison can be done with confidence is selected from members of the cluster M67. For this cluster D. Latham and S. Meibom provided a list of 116 stars

that are thought to be single cluster members. We estimated T_{eff} and $\log(g)$ for these stars from a fit to the Yi et al. (2008) isochrone for solar metallicity and an age of 4 GY. Note that M67 lies far outside the *Kepler* field of view, so these stars do not appear in the KIC proper. Figure 7a shows the comparison between T_{eff} values for M67 estimated from the KIC and those from a stellar evolution model fit to Montgomery’s B,V photometry (Montgomery et al. 1993). With the exception of two extreme outlying stars, the agreement is generally good. The *RMS* difference between the measurements is about 150 K, and the systematic differences appear to be small. Figure 7b shows the analogous comparison for $\log(g)$. Again the general agreement is good, with an RMS difference between the isochrone measurements and the KIC fits of about 0.4 dex. Systematic differences are discernible in $\log(g)$, however. The most significant of these is a tendency for subgiants identified via isochrone fitting appear as main-sequence stars in the KIC analysis. This is not surprising, since in the T_{eff} range where the turnoff to the subgiant branch occurs in M67, none of the filter combinations that were observed for the KIC are sensitive to gravity. The color ($g - D51$) shows a useful gravity dependence only for ($g - r$) colors greater than 0.65, whereas the main-sequence turnoff in M67 lies at bluer colors, roughly ($g - r$) = 0.38.

10.4. Comparisons with spectroscopic parameter estimates

We and others have made comparisons between KIC estimates of stellar parameters and various sets of parameters estimated from modeling of optical spectra.

Molenda-Zakowicz et al. (2010) obtained spectra for 109 relatively bright KIC stars, spanning a wide range of T_{eff} . They found that for temperatures below 7000 K, KIC T_{eff} values agree with their spectroscopic estimates within about ± 200 K, but that at higher temperatures, larger deviations occur. The largest errors appear for the hottest stars; indeed, in this sample there are 9 stars with spectroscopic T_{eff} values in the range 9000

K to 13500 K, and all of these stars are shown in the KIC with lower temperatures, with differences as large as 4000 K. As mentioned above, these failures of temperature estimation are expected for hot stars, because of the absence of u -band data. Molenda-Zakowicz et al. (2010) found that the KIC surface gravity estimates were fairly accurate for dwarfs, but for giants (including those with $\log(g)$ as low as 1.5), the KIC estimates could be in error, sometimes by as much as 1.5 dex.

In the process of studying candidate planet host stars, the *Kepler* mission has obtained high signal-to-noise Keck/HIRES spectra of a few tens of stars, and D. Fischer has analyzed these with the Spectroscopy Made Easy (SME) package (Valenti & Piskunov 1996) to estimate their values of T_{eff} , $\log(g)$, and $[\text{Fe}/\text{H}]$. Figure 8a shows the comparison for all 3 parameters for 34 of these stars (all that were available as of Sep. 2010). The selection criteria for these *Kepler* planet candidates assured that this sample of stars consists almost entirely of dwarfs with roughly solar T_{eff} . Thus, the T_{eff} range is considerably smaller than for the sample measured by Molenda-Zakowicz et al. (2010). For all but 2 of these stars, the difference between KIC and HIRES/SME values of T_{eff} is 200 K or less; the RMS difference is 135 K. There is some evidence for a systematic trend in the T_{eff} differences, with the KIC temperatures being cooler than Keck/HIRES at low T_{eff} and warmer at high T_{eff} , but more measurements are needed to confirm this impression. Figure 8b compares the KIC and HIRES/SME estimates of $\log(g)$. Except for one star (spectroscopically classified as a subgiant with $\log(g) = 3.5$), the two sets of estimates agree within ± 0.3 dex, and the RMS difference is only 0.25 dex. We consider that this agreement is largely artificial, however. The *Kepler* planetary transit candidates consist almost entirely of stars classified as dwarfs in the KIC, and hence included in the *Kepler* target list. If these stars are observed to show photometric transit events, then the original classification is likely correct. Thus, for stars selected as these were, we expect at least rough agreement concerning $\log(g)$. Figure 8c compares the KIC and HIRES/SME values of $[Z]$ for the same stars (excluding a few

stars in the previous plots for which HIRES/SME values of $[Fe/H]$ were not reported). The total range of $[Fe/H]$ estimated by HIRES/SME for these stars is small, about 0.7 dex, and most of the stars are clustered in about half of this range. Accepting (for lack of an alternative) the shortcomings of this sample, one finds that the RMS difference between the two sets of estimates is 0.2 dex, and that the Spearman rank correlation coefficient is 0.42, with a two-sided significance of its deviation from zero of 0.02. For comparison, the Spearman statistics for the different T_{eff} measurements are 0.96 and 5×10^{-17} , respectively. Thus, while there is evidence that the KIC values of $[Z]$ are related to those measured spectroscopically, the strength of this relationship is unimpressive. Moreover, there appears to be a significant systematic difference between the KIC and HIRES/SME values, in the sense that the KIC $[Z]$ values are about 0.17 dex smaller. We suspect this is symptomatic of the Bayesian prior for $[Z]$ being rather narrowly peaked around $[Z] = -0.1$, whereas planet-bearing stars (which are abundant in this sample) are typically metal-rich (e.g, Fischer & Valenti (2005)).

The *Kepler* mission has also observed a much larger sample of stars using relatively low signal-to-noise ratio spectroscopy (S/N of typically 7 to 10) obtained from several different sources (McDonald 2.7m, Mt. Hopkins 1.5m, Lick 3m, and Nordic Optical Telescope 2.5m telescopes). These spectra were obtained to facilitate identification of stellar binaries and to provide crude spectral classifications, so as to make an early decision about the likely origin of apparent photometric transit signals. These “reconnaissance” spectra were analyzed by correlating them against templates created from stellar atmosphere models, using a grid spacing of 250 K in T_{eff} and 0.5 dex in $\log(g)$, and assuming solar metallicity. The stars in this sample were commonly observed spectroscopically 2 or 3 times each. Again, by virtue of being selected as transiting planet candidates, these stars form a biased sample, favoring dwarfs. In Figure 9 we plot the average (over observations) of the T_{eff} and $\log(g)$ values estimated for each star against the similar values found in the KIC.

The agreement between KIC classifications and the ones from reconnaissance spectroscopy are worse than for the KECK/HIRES/SME classifications, with random T_{eff} differences of about 360 K RMS, random $\log(g)$ differences of roughly 0.3 dex, and evidence for systematic errors of similar magnitude. On the other hand, comparisons between successive spectroscopic estimates of T_{eff} and $\log(g)$ for any given star show scatter of similar size. Thus, a substantial fraction of the scatter in Figure 9 likely results from errors in the spectroscopic reconnaissance measurements. Improved analysis techniques for reconnaissance spectroscopy will soon provide better material for assessing errors in the KIC. In the meantime, we find that KIC T_{eff} and $\log(g)$ estimates agree with those from reconnaissance spectroscopy about as well as the latter agree with each other.

10.5. Comparisons with asteroseismic parameter estimates

Many stars with KIC classifications have been observed to oscillate in global modes, usually p-modes. Indeed, early *Kepler* observations are the source of the vast majority of these pulsation detections.

In a simple test, Koch et al. (2010) compared the RMS photometric variability of 1000 stars with $T_{\text{eff}} \leq 5400$ K, that the KIC classifies as giants, with an equal number classified as dwarfs. Giants are known to be systematically more variable, because virtually all of them show p-mode oscillations with amplitudes that increase with increasing stellar luminosity. In these samples, about 2.5% of the stars classified as dwarfs showed variability consistent with their being giants, and none of those classified as giants had variability consistent with dwarfs. It thus appears that, averaged over this sample, the KIC is more than 98% successful in its principal aim – to distinguish between cool giant and dwarf stars.

Detailed seismic analyses have been published for a few Sun-like dwarfs in the *Kepler*

field. Christensen-Dalsgaard et al. (2010) used *Kepler* time series to search for p-mode frequencies and estimate stellar parameters in 3 *Kepler*-field stars that were known from groundbased observations to host transiting planets. All of these stars (HAT-P-7, HAT-P-11, and TrES-2) are however too bright to avoid saturation in the SCP photometry, hence have no T_{eff} or $\log(g)$ values in the KIC. Chaplin et al. (2010) analyzed *Kepler* time series for 3 fainter Sun-like stars, namely KIC 6603624, 3656476, 11026764. The analysis included groundbased high-resolution spectroscopy (allowing estimates of T_{eff} , $\log(g)$, and $\log(Z)$), and p-mode fitting, which when combined with the non-seismic data, allowed estimates of the stellar mass and radius. For these stars, the KIC estimates of T_{eff} were all lower than the spectroscopic ones, by $\{-374 \text{ K}, -242 \text{ K}, -138 \text{ K}\}$ respectively. The KIC estimates of $\log(g)$ were all larger than the seismic estimates, by $\{0.064, 0.253, 0.066\}$ dex, respectively. Metcalfe et al. (2010) did an independent analysis of KIC 11026764, finding T_{eff} and $\log(g)$ values that are consistent with those by Chaplin et al. (2010).

Early *Kepler* data have revealed long-lived p-modes in a large number of giant stars. A recent study by Hekker et al. (2011) has made an explicit comparison between KIC and asteroseismic estimates of $\log(g)$ for a sample of 11805 stars classified as giants in the KIC that also have Quarter-0 and Quarter-1 *Kepler* time series available to the public, and in which p-modes have been detected. These authors used the method described by Kallinger et al. (2010) to estimate stellar masses and radii from the p-mode large frequency separation $\Delta\nu$, the frequency of maximum power ν_{max} , and the KIC estimate of T_{eff} . This comparison shows that while the KIC correctly ascribes low surface gravities ($\log(g) \leq 3.8$) to almost all of these stars, the KIC values are systematically too large relative to the asteroseismic ones. The magnitude of this error is larger for lower gravities; for clump giants, with $2.3 \leq \log(g) \leq 2.7$, it is about 0.5 dex. The KIC values also show larger scatter at given T_{eff} than do the asteroseismic ones.

10.6. Comparison with *Hipparcos* Parallaxes

For a small sample of stars, one may usefully compare the distances inferred from the KIC analysis with parallaxes measured by the *Hipparcos* mission (Høg et al. 2000). As described in §7, the distance d to an observed star is implied by its apparent r magnitude, its galactic latitude, and the exponential model that we use for interstellar extinction. The distance d is not tabulated in the KIC, but it may be computed from the (tabulated) V -band extinction A_V as

$$d = -\frac{h}{\sin b} \ln\left(1 - A_V \frac{\sin b}{k_V h}\right), \quad (20)$$

where h is the dust scale height (assumed to be 150 pc), b is the galactic latitude, and k_V is the dust opacity in the galactic plane (assumed to be 1 mag pc⁻¹).

Unfortunately, stars with reliable ($\pm 20\%$) *Hipparcos* distances tend to be brighter than typical stars with valid (not saturated) SCP photometry. Thus, the number of stars having both 20%-accurate *Hipparcos* parallaxes and converged parameter solutions is only 55, and these lie at distances that are considerably smaller than those of typical *Kepler* stars. Figure 10 shows the comparison of parallax *vs* extinction distances for this sample of stars. These stars span magnitudes $7.88 \leq r \leq 10.84$, with colors $-0.47 \leq g - r \leq 0.87$, and KIC temperatures $4684 \text{ K} \leq T_{\text{eff}} \leq 10735 \text{ K}$. The absolute magnitudes we compute for these stars (based on the parallaxes) show that all but 2 lie on the main sequence. About 65% of these stars have parallax- and extinction-based distances that agree within a factor of 1.7, or ± 0.23 dex. Little of this scatter can be attributed to the parallaxes, so this comparison suggests that KIC stellar radii have $1\text{-}\sigma$ errors that are also about 0.2 dex. This is roughly consistent with our previous estimate of 0.4 dex for the typical error in $\log(g)$.

Figure 10 also suggests that (aside from 2 dramatic outliers) the extinction distances are systematically too small. For this sample of stars, the median distance error is -0.12 dex, or a factor of 0.76. There are two possible explanations for this bias: the in-plane

dust opacity k_V may be overestimated, or the luminosities that we attribute to dwarf stars may be too small. We believe that too-small luminosities are mostly at fault, since this explanation is consistent with our previous conclusion that we tend to overestimate $\log(g)$ for dwarfs.

There are also 2 stars for which the extinction distances are much too large. One of these is a binary G-type dwarf that the KIC evidently misclassified as a giant, giving a distance that is much too large and $\log(g)$ that is much too small. The other, HIP93941 = BD+42°3250, is classified by Catanzaro et al. (2010) as a B2 star with weak He lines, and by Østensen et al. (2010) as an sdB star. Thus, its temperature is surely much hotter than the KIC value of 10735 K, and its parallax yields $V_{abs} = 4.4$. This stellar class is not represented in the Bayesian prior distribution used in the KIC analysis, and hence the object was misclassified as a more luminous and distant star than it actually is.

11. KIC Shortcomings

As indicated above, the stellar classifications provided in the KIC suffer from several known systematic defects that should be considered when using the catalog. Here we describe (or repeat) the most important of these, explain their source when this is known, and illustrate the problems with samples from the data.

11.1. T_{eff} Scale

KIC T_{eff} values have systematic disagreements with other T_{eff} estimates that apply to the same stars. (Of course, these other estimates also disagree systematically with each other.) For approximately Sun-like stars these disagreements are usually less than 50K, though in the worst cases they may exceed 200K. For stars that are distant from the Sun

on the CMD, one must be more cautious. The KIC T_{eff} estimates are untrustworthy for $T_{\text{eff}} \geq 10^4\text{K}$, and also for $T_{\text{eff}} \leq 3750\text{K}$.

For hot stars ($T_{\text{eff}} \geq 9000\text{K}$), the lack of u -band data makes our photometry insensitive to variations in T_{eff} . Higher temperatures are found in the KIC estimates, but their values should not be trusted. We used a subset of the CK models with a maximum T_{eff} of 19,000K; the absence of estimates above this value therefore does not imply the absence of such stars in the sample.

The CK model atmospheres we used covered only $T_{\text{eff}} \geq 3500\text{K}$, and we applied ad hoc corrections to the colors for $T_{\text{eff}} \leq 3750\text{K}$. Temperatures below the latter value are therefore also questionable (although at fixed composition and gravity, the KIC T_{eff} is probably at least a monotonic function of the true T_{eff}).

11.2. Subgiant gravity

The KIC classifications tend to give $\log(g)$ too large for subgiant stars, especially those hotter than about 5400K. This leads to underestimates of the radii of this subset of stars, typically by factors of 1.5 to 2.

For temperatures above roughly 5400K, none of our photometric colors provide information about surface gravity. Accordingly, for hotter temperatures the maximum posterior probability analysis has no basis to choose any $\log(g)$ other than the one that is most probable a priori, which corresponds to the center of the main sequence, near $\log(g) = 4.5$. Stars on the giant branch almost all have T_{eff} small enough so that their gravities can be measured; so the gravities of true giants appear to be estimated with errors of typically about 0.5 dex. But for a significant subset of (mostly hot) stars, the KIC-derived gravities are systematically too large, sometimes by more than 1 dex.

Given the available photometric data, this problem is essentially unavoidable. The information needed to distinguish between F- and early G-type dwarfs and subgiants is not present in the photometry, and there is no way to obtain sensible results without it. (Biasing the prior probabilities towards lower gravities, for instance, results in more subgiants, but with no guarantee that the new alleged subgiants are in fact the stars with low gravity.) Users should thus be wary of $\log(g)$ estimates for $(g - r) \leq 0.65$.

11.3. High $\log(Z)$ at low T_{eff}

We could perform few tests of the veracity of the estimates of $\log(Z)$, and (given the absence of u -band magnitudes) there is little reason to trust these estimates. The $(g - D51)$ color contains information about $[Z]$, but this is almost entirely degenerate with the larger and more common color perturbation caused by surface gravity.

A plot of $\log(Z)$ vs $\log(T_{\text{eff}})$ for a large randomly-sampled group of stars (Figure 10) shows a number of peculiarities. For T_{eff} below about 4200K ($\log(T_{\text{eff}}) = 3.623$), the estimated $\log(Z)$ distribution begins to spread and bifurcate, and below 3800K ($\log(T_{\text{eff}}) = 3.580$), virtually all stars show $\log(Z)$ greater than +0.5, which is the highest metallicity represented in the CK models that we use. This behavior has not been investigated in detail, but it seems likely that it results from a mismatch between the model and observed color dependences at low temperatures, in the sense that (other astrophysical evidence notwithstanding), high-metallicity stars provide the best fit to the observations.

One can also observe clustering of $\log(Z)$ around integral and half-integral values of $\log(Z)$, for $\log(Z) \leq -1$. These are the tabulated values of $\log(Z)$; the concentration of estimated values near the tabulated ones presumably indicates a failure of the interpolation and fitting code that optimizes the posterior probability.

The most encouraging demonstration that the estimates are doing something sensible was provided by the classifications of stars in the globular clusters M13 and M92. These clusters showed a fairly large (but by no means dominant) fraction of low- Z star classifications. Based on their positions in our observed cluster color-magnitude diagrams, all of these cluster stars were, however, cool giants, for which we suspect the model colors are particularly uncertain. Thus, whether the classifications for metallicity are performing properly for main-sequence stars is unknown at present; it would be prudent to assume that they are not. Fortunately, the fraction of low-metallicity stars in the solar neighborhood is quite small, so for the purposes of the *Kepler Mission* the uncertainty about $\log(Z)$ is tolerable. But anyone with a particular interest in stellar metallicities should not use the KIC for their estimates of $\log(Z)$.

11.4. Extinction and Reddening

Regions at low galactic latitude are prone to have large and spatially nonuniform extinction and reddening. The model of extinction that is employed in the Bayesian posterior probability maximization contains no small-scale structure, so it is unable to deal properly with localized large deviations from the mean extinction. The result is systematic misclassification of many stars, a scattered and confused relation between T_{eff} and color, and other failings. Examples of such difficulties are shown in Figure 11, which compares tiles at low and high galactic latitudes.

12. Summary and Conclusions

The *Kepler* Input Catalog is available via the MAST archive facility, operated by the Space Telescope Science Institute ³.

Experience with the KIC, combined with the testing that we report here and that has been done elsewhere, shows that the KIC has succeeded in its primary goal – to distinguish between cool giant and dwarf stars with good reliability, so that the *Kepler Mission* can select optimum targets for its transiting-planet search. As a by-product of that goal, the KIC provides photometry in the SDSS-like photometric bands g, r, i, z and in the intermediate-bandwidth $D51$ bandpass, calibrated with a typical flux accuracy of about 2%, for stars brighter than about magnitude 14 in any of our filters. All of this information is federated with that from other key photometric and astrometric databases, so that the KIC can serve as a tool for research on a great number of objects that will not be observed by *Kepler* itself.

Experience and testing has also shown that the KIC has defects. The most notable of these include stars that appear in other catalogs but that have no physical classifications in the KIC, systematic errors in estimates of T_{eff} for hot and for very cool stars, systematic errors in estimates of $\log(g)$ for stars with $g - r$ colors that are bluer than about 0.65, and questionable metallicity determinations across the CMD. Most of these problems arise from a common cause, namely lack of information about the desired physics in the mostly wideband photometry that we were able to obtain. By combining u -band, and perhaps also suitable intermediate-bandwidth observations with the techniques described here, it should be possible to extend greatly the T_{eff} range over which the KIC parameter estimates are reliable, and to improve substantially the KIC's metallicity sensitivity. Also,

³<http://archive.stsci.edu/kepler/kic10/search.php>

careful spectroscopic observations of stars that have KIC classifications should allow better characterization of the KIC’s systematic errors. We hope that others will find it useful to provide these improvements.

We are grateful to the Mt. Hopkins support and observing staff, especially Carl Hergenrother, for his tireless work obtaining the necessary observations. We also thank Dave Monet, for his indispensable help in implementing the KIC astrometry methods, and for federating the SCP with other catalogs that carry essential information. We thank Steve Howell, for helping to define our photometric approach in the project’s early days. We thank Geoff Marcy, Howard Isaacson, Debra Fischer, Bill Cochran, Sam Quinn, Lars Buchhave, Mike Endl, and Phillip MacQueen for the use of their spectra and spectral analysis of *Kepler* target stars. We also thank Saskia Hekker, Bill Chaplin, Ronald Gilliland, and dozens of members of the *Kepler* Asteroseismic Consortium for making their seismic data available before publication. We are deeply grateful to the *Kepler* Science Team and everyone connected with the *Kepler Mission*, for keeping the mission running smoothly, and for providing the amazing *Kepler* photometric data, the promise of which was the inspiration for the current work. We thank Jeffrey Scargle for a careful reading of an early version of this work, and Don Kolinski for extensive software development help. T.B. acknowledges support from NASA Grant Number NNX10AG02A, and thanks HAO/NCAR and Las Cumbres Observatory Global Telescope for patience and support while this work was being done. The National Center for Atmospheric Research is supported by the National Science Foundation. We are grateful to the *Kepler Mission* for partial support of the photometric observations under NASA Cooperative Agreement NCC-1390 with the Smithsonian Astrophysical Observatory.

REFERENCES

- Abazajian, K., et al. 2003, *AJ*, 126, 2081
- Abazajian, K., et al. 2004, *AJ*, 128, 502
- Bessell, M. S., & Brett, J. M. 1988, *PASP*, 100, 1134
- Borucki, W. J., et al. 2010, *Science*, 327, 977
- Cardelli, J. A., Clayton, G. C., & Mathis, J. S. 1989, *ApJ*, 345, 245
- Castelli, F., & Kurucz, R. L. 2004, arXiv:astro-ph/0405087
- Catanzaro, G., Frasca, A., Molenda-Żakowicz, J., & Marilli, E. 2010, *A&A*, 517, A3
- Chaplin, W. J., et al. 2010, *ApJ*, 713, L169
- Christensen-Dalsgaard, J., et al. 2010, *ApJ*, 713, L164
- Cox, A. N. 2000, *Allen’s Astrophysical Quantities*, 4th Ed., New York: AIP Press; Springer, A.N. Cox, ed.
- ESA 1997, “The Hipparcos and Tycho Catalogues”, ESA SP-1200
- Fischer, D. A., & Valenti, J. 2005, *ApJ*, 622, 1102
- Fukugita, M., Ichikawa, T., Gunn, J. E., Doi, M., Shimasaku, K., & Schneider, D. P. 1996, *AJ*, 111, 1748
- Girardi, L., Bressan, A., Bertelli, G., & Chiosi, C. 2000, *A&AS*, 141, 371
- Hekker, S. et al. 2011, *MNRAS*(submitted)
- Høg, E., et al. 2000, *A&A*, 355, L27

Kallinger, T. et al. 2010 *A&A*, 509, A77

Koch, D.G. et al. 2010, *ApJ*, 713, L79

Koppen, J., & Vergely, J.-L. 1998, *MNRAS*, 299, 567

Lejeune, T., Cuisinier, F., & Buser, R. 1997, *A&AS*, 125, 229

Marshall, D. J., Robin, A. C., Reylé, C., Schultheis, M., & Picaud, S. 2006, *A&A*, 453, 635

Metcalfe, T. S., et al. 2010, *ApJ*, 723, 1583

Molenda-Zakowicz, J., Jerzykiewicz, M., Frasca, A., Catanzaro, G., Kopacki, G., & Latham,
D. W. 2010, arXiv:1005.0985

Monet, D. G., et al. 2003, *AJ*, 125, 984

Montgomery, K. A., Marschall, L. A., & Janes, K. A. 1993, *AJ*, 106, 181

Nordström, B., et al. 2004, *A&A*, 418, 989

Oke, J. B. 1974, *ApJS*, 27, 21

Østensen, R. H., et al. 2010, *MNRAS*, 409, 1470

Perryman, M. A. C., et al. 1997, *A&A*, 323, L49

Sandquist, E. L. 2004, *MNRAS*, 347, 101

Skrutskie, M. F., et al. 2006, *AJ*, 131, 1163

Smith, J. A., et al. 2002, *AJ*, 123, 2121

Stetson, P. B. 1987, *PASP*, 99, 191

Stetson, P. B., Bruntt, H., & Grundahl, F. 2003, *PASP*, 115, 413

Stoughton, C., et al. 2002, AJ, 123, 485

Stoughton, C., & Jester, S. 2004, AGN Physics with the Sloan Digital Sky Survey, 311, 475

Valenti, J. A., & Piskunov, N. 1996, A&AS, 118, 595

Yi, S. K., Kim, Y.-C., Demarque, P., Lee, Y.-W., Han, S.-I., & Kim, D. G. 2008, IAU
Symposium, 252, 413

Zacharias, N., Urban, S. E., Zacharias, M. I., Wycoff, G. L., Hall, D. M., Monet, D. G., &
Rafferty, T. J. 2004, AJ, 127, 3043

Figure Captions

Fig. 1.— The combined atmospheric and instrumental coefficients a_i (see Eqn 1) for the g , $D51$, r , i , and z filters for 203 of the 205 nights on which KIC data were obtained. The remaining 2 nights gave values that are extreme outliers, falling outside the range of these plots. Zero points on these curves have been shifted for plotting convenience. Note the color dependence of the temporal variations, which tend to be larger in blue filters than in red. Vertical dashed lines indicate the dates of transition between CCD cameras.

Fig. 2.— Plot of g extinction data on a representative (mildly non-photometric) night. The top panel shows extinction as a function of airmass. Points plotted as diamonds were obtained before the meridian transit of the standard star field; those plotted as triangles were obtained after it. Vertical bars indicate the interquartile spacing of results from the 20 stars used to estimate the extinction. The diagonal dashed line is the result of a robust linear fit to the extinction values, with coefficients tabulated in the upper left corner of the plot. The bottom panel shows residuals around this fit plotted against the time-varying FWHM of the stellar point spread function.

Fig. 3.— Variation in the k_i coefficient (extinction per unit airmass in the i^{th} filter), shown as a function of date, for nights for which reliable linear fits to the extinction could be obtained, during a part of one observing season. The time span shown here was one of the most variable that we encountered in 5 seasons of observing, but is nonetheless typical in its variability within a factor of 1.5. Filters g , $D51$, r , i , z are shown in order from top to bottom of the plot. Night-to-night variations tend to be not only correlated, but of similar size among the filters. An exception is the z filter, in which the extinction is evidently affected by a different process than at shorter wavelengths. We believe that this process is extinction from water vapor.

Fig. 4.— Photometric repeatability for stars in the secondary standard fields, after correction for atmospheric extinction for each filter, shown as a function of apparent magnitude in that filter.

Fig. 5.— Comparison between observed and model colors. This plot represents all of the stars contained in one tile, covering an area spanning 1 degree in RA by 1 degree in Dec on the sky near galactic latitude $b \simeq 10.5^\circ$. Each point corresponds to one star, and the plotted positions show the residuals (in magnitudes) after subtracting the best-fit model from the photometry for that star, for two chosen colors (eg $g - i$ vs $g - r$, as in panel a). Different panels show various combinations of colors, indicated in the axis labels. The tile plotted here (at RA=292° and Dec =+40°) is fairly typical of areas in which the model fits are good. There are several notable features. In panels a and b, the *RMS* scatter in the residuals is .02 mag or less in each of $g - r$, $r - i$, and $g - D51$. Errors are anticorrelated between $g - r$ and $g - i$, but this tendency is more noticeable and has a different slope in the wings of the distributions than in the cores. In panels c and d, note the larger scatter (especially in $z - J$, and also the strong negative correlations between these pairs of residuals. In panels e and f, note the change in plot scale; the residuals in the IR colors are much larger than in the visible bands. The $J - K$ and $g - i$ residuals are almost uncorrelated, but one now sees a very significant offset from zero of the mean residual in $g - i$. The two IR colors in the bottom panel have only slightly correlated residuals, but the center of the $J - H$ distribution is also far displaced from zero.

Fig. 6.— Panel (a) shows the $(g - D51)$ vs $(g - r)$ color-color diagram for the same 1-degree-square tile as shown in the previous Figure, at galactic latitude $b \simeq 10.5^\circ$. Stars classified as giants (with $\log g < 3.6$) are indicated by red symbols, and dwarfs (with larger $\log(g)$) are plotted in black. Panel (b) is similar to the above, but shows a $(J - K)$ vs $(g - i)$ color-color diagram for the same tile. The meaning of the symbols is the same.

Fig. 7.— Stellar parameter estimates for confirmed single stars in the star cluster M67. Estimates from the KIC are plotted on the y -axis; along the x -axis are values from the 4 GY solar-abundance Yonsei-Yale isochrone (Yi et al. 2008), fit to B,V photometry by Montgomery et al. (1993). The diagonal dashed line indicates equality. Panel (a) shows T_{eff} on each axis, with lines showing equality and ± 200 K overplotted. Panel (b) similarly shows $\log(g)$, with lines showing equality and ± 0.3 dex.

Fig. 8.— Parameter estimates from the KIC plotted against estimates by D. Fischer from SME model spectrum fitting, for stars observed with the Keck/HIRES spectrometer as possible transiting planet hosts. A few stars have more than one independent HIRES/SME observation and analysis; in these cases the various results are shown connected by horizontal lines. Panel (a) shows T_{eff} on each axis, with lines showing equality and ± 200 K overplotted. Panel (b) shows $\log(g)$, with lines showing equality and ± 0.3 dex. Panel (c) similarly shows $\log(Z)$, with line showing equality and ± 0.4 dex.

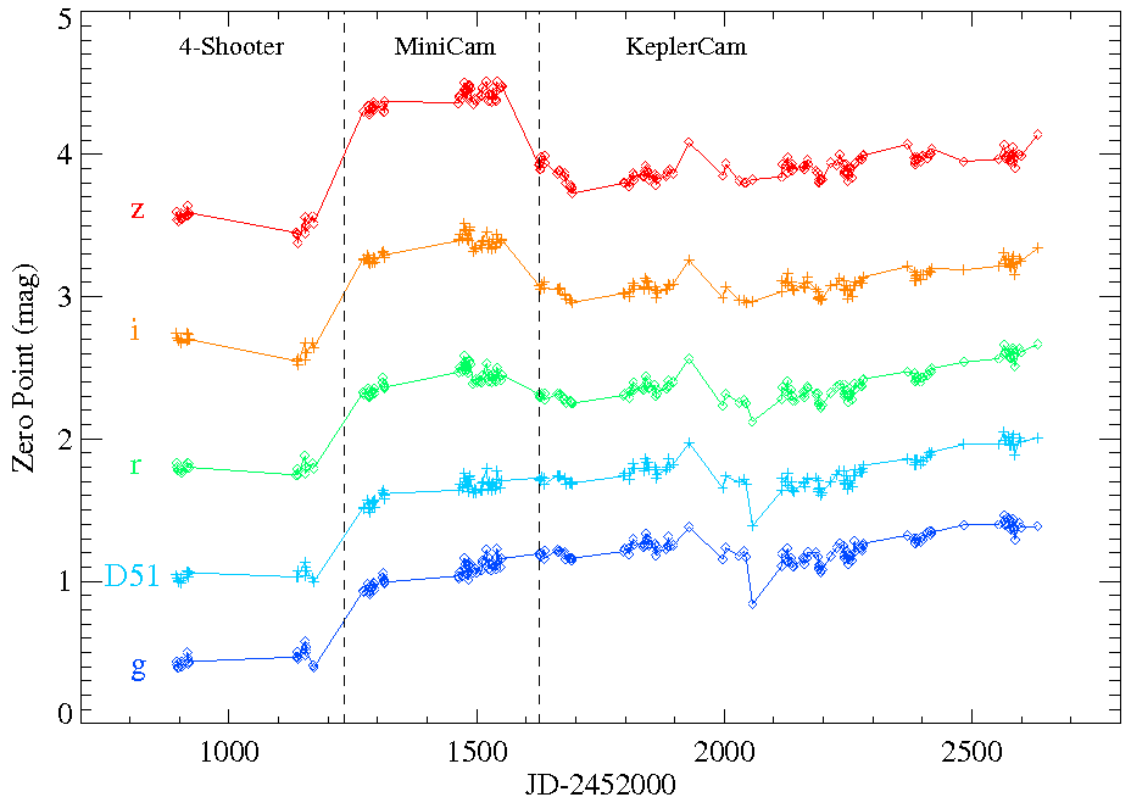
Fig. 9.— Same as the previous Figure, except for stars with T_{eff} and $\log(g)$ estimates from matching a grid of models to reconnaissance spectroscopy of *Kepler* transiting planet candidates. Most plotted points are the average of results from 2 or more independent spectra. Also, small random offsets have been applied in both axes, to reduce crowding. Diagonal lines indicate equality and ± 250 K, ± 0.3 dex. The analysis of these spectra provided no metallicity estimates, so $\log(Z)$ is not shown.

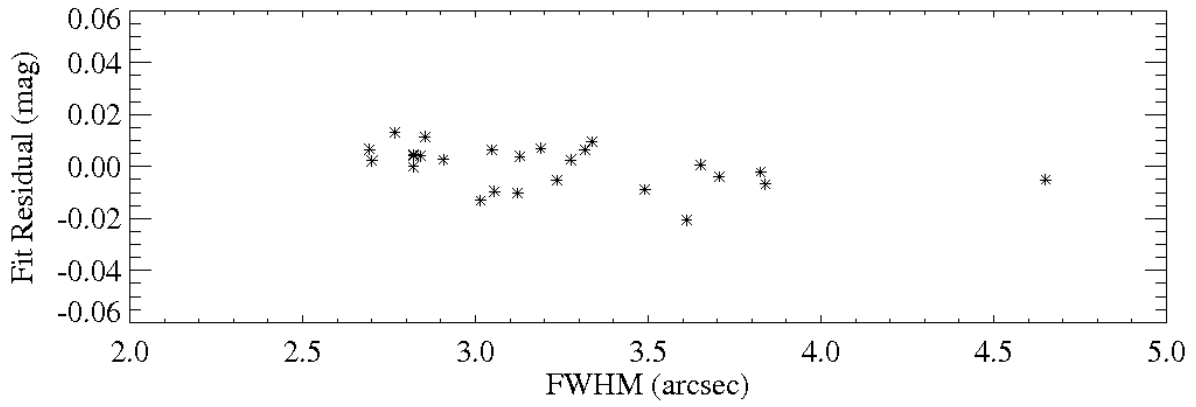
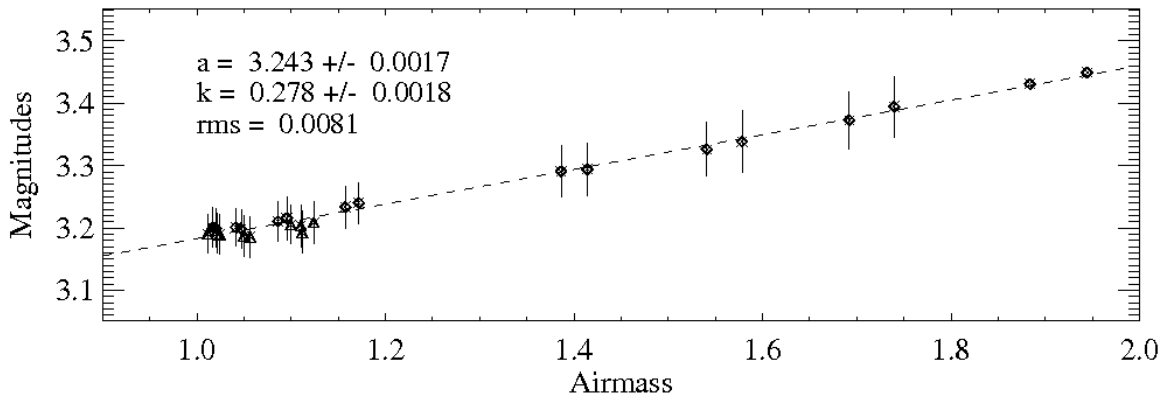
Fig. 10.— Comparison between KIC “Extinction” distances and *Hipparcos* “Parallax” distances to stars in the Kepler field, having valid KIC stellar parameters and parallaxes accurate to 20% or better. Error bars correspond to $\pm 1\text{-}\sigma$ uncertainties on the parallaxes. Diagonal lines indicate equality and ± 0.23 dex (factor of 1.7).

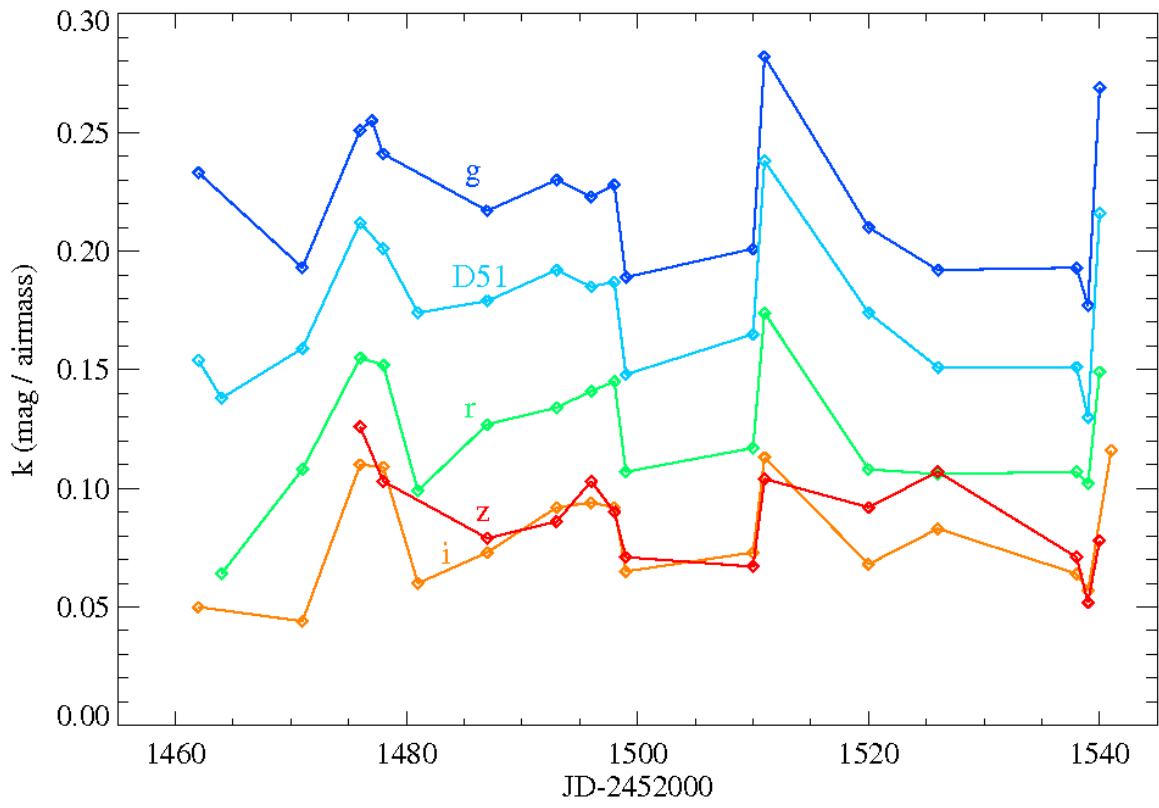
Fig. 11.— Plot of KIC estimates of $\log(Z)$ against $\log(T_{\text{eff}})$, illustrating the strong tendency

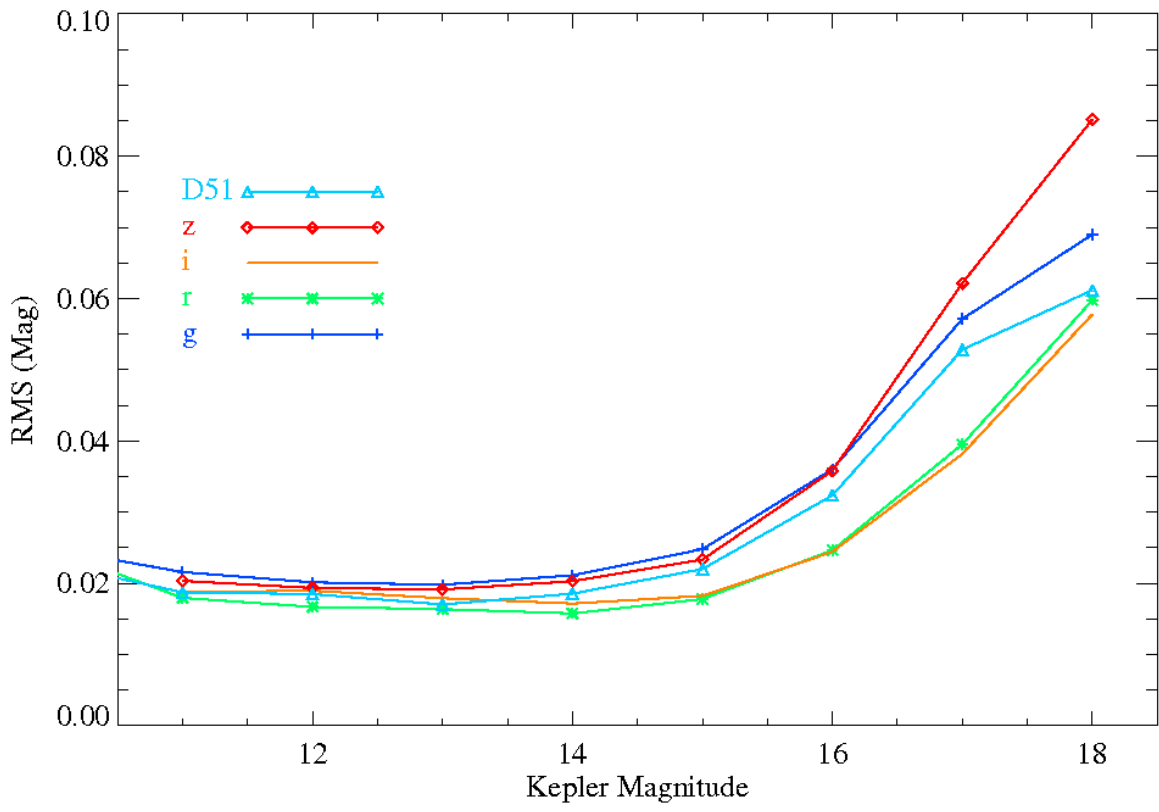
of low-temperature stars to be classified with high metallicity, and moreover the tendency for low- Z stars to be ascribed integral- or half-integral values of $\log(Z)$, independent of T_{eff} .

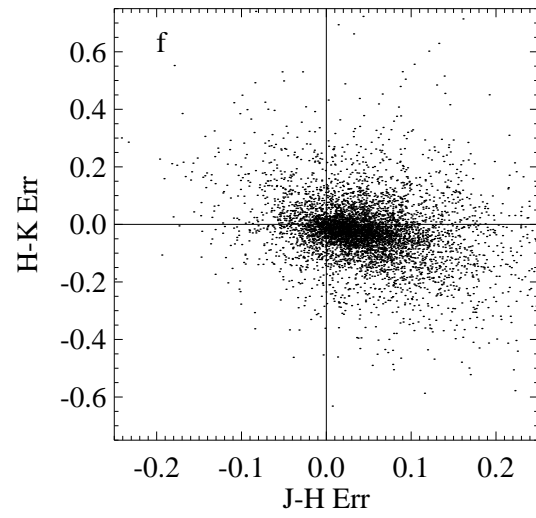
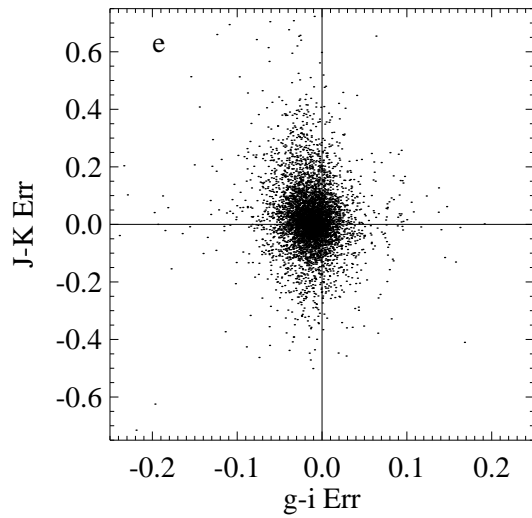
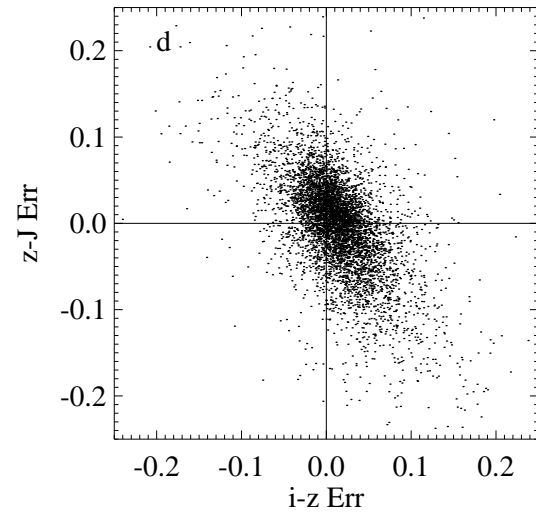
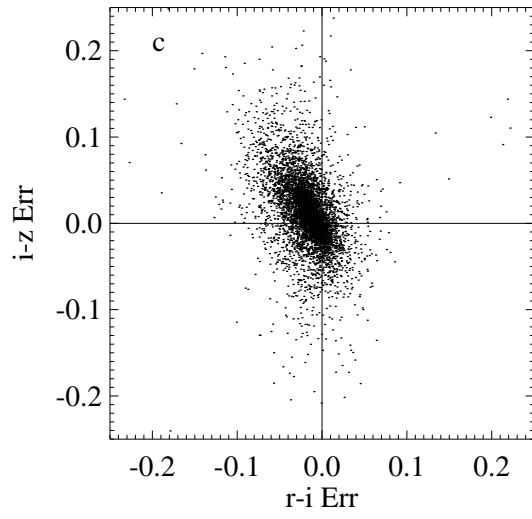
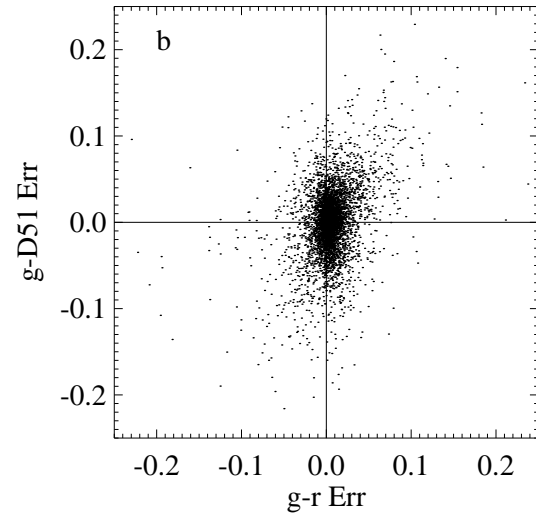
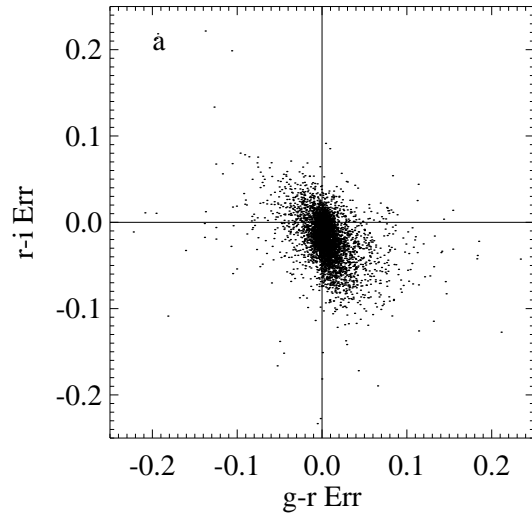
Fig. 12.— The relation for $(g-r)$ color (uncorrected for interstellar reddening) and $\log(T_{\text{eff}})$, for a tile near the galactic plane, at $b \simeq 6^\circ$ (panel a), and at $b \simeq 18^\circ$ (panel b). Besides having more stars per unit area near the plane, the near-plane scatter diagram shows general reddening, increased spread in color at each T_{eff} , and a complex, roughly bimodal structure.

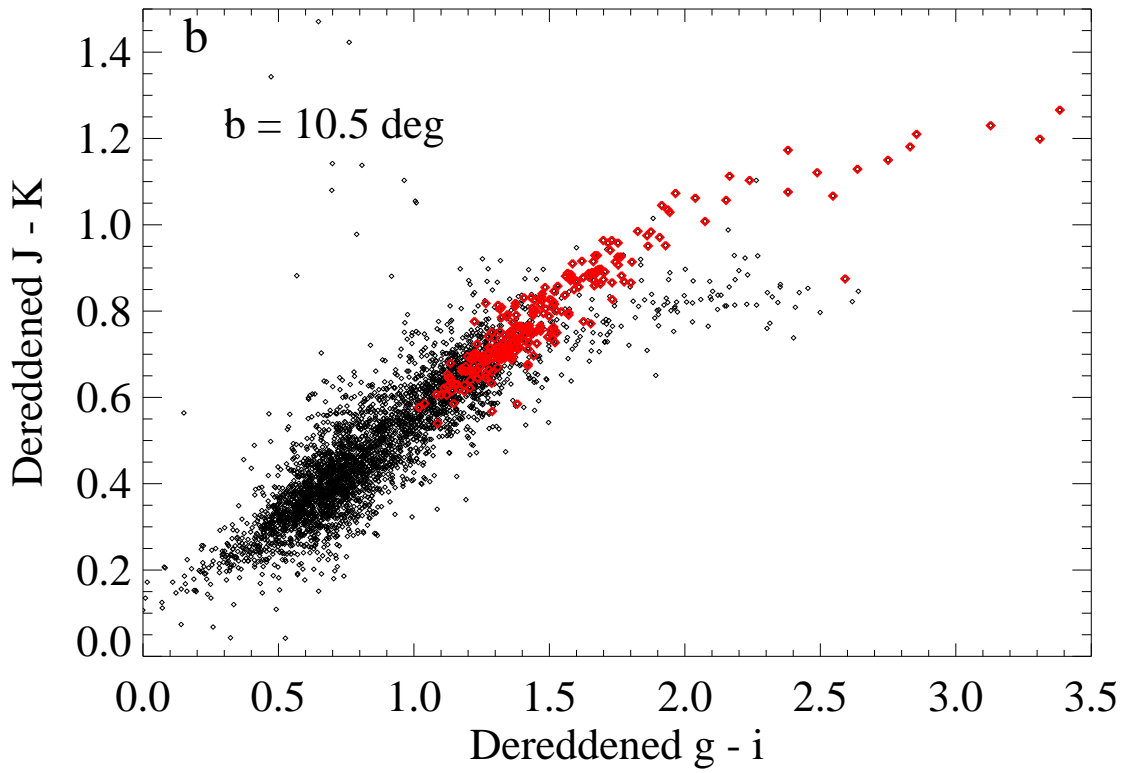
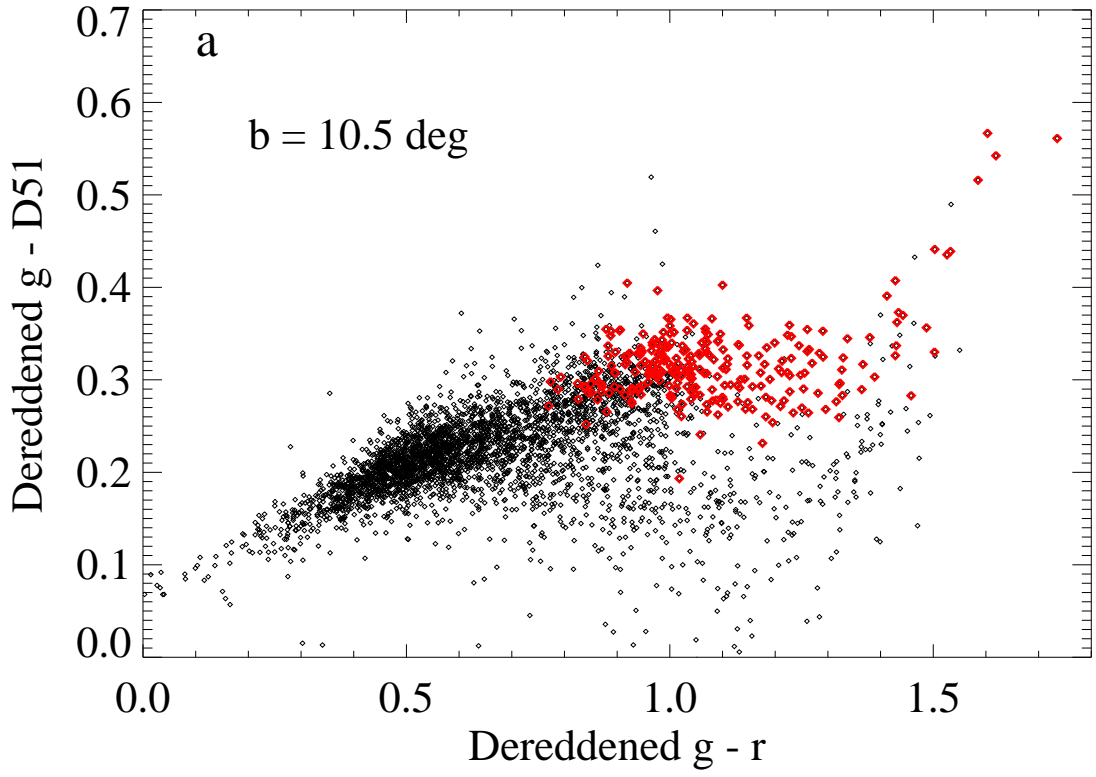


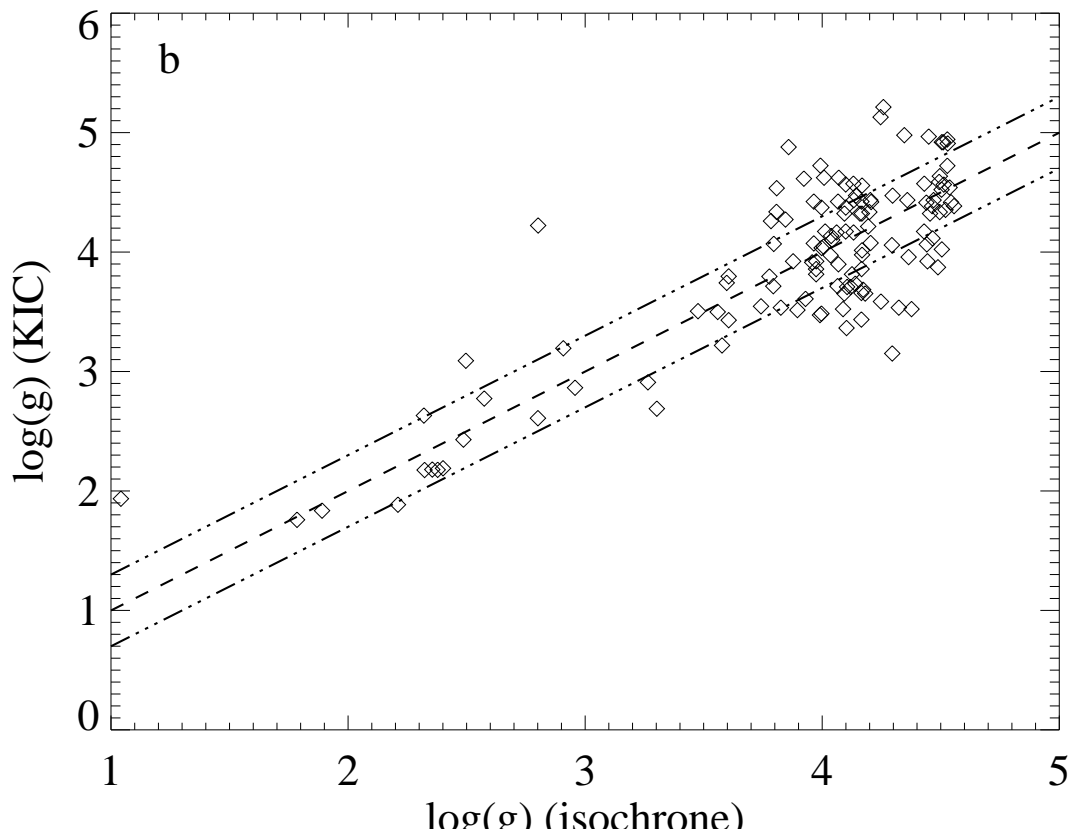
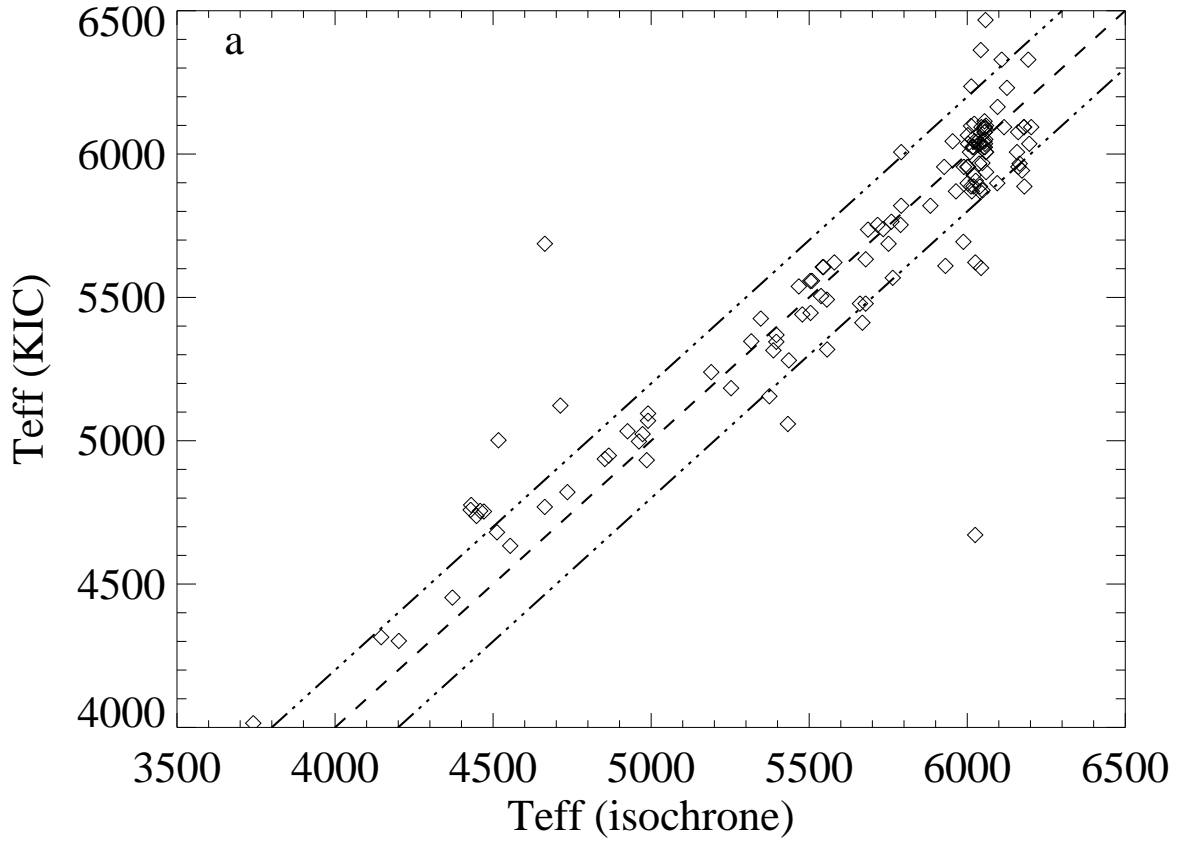


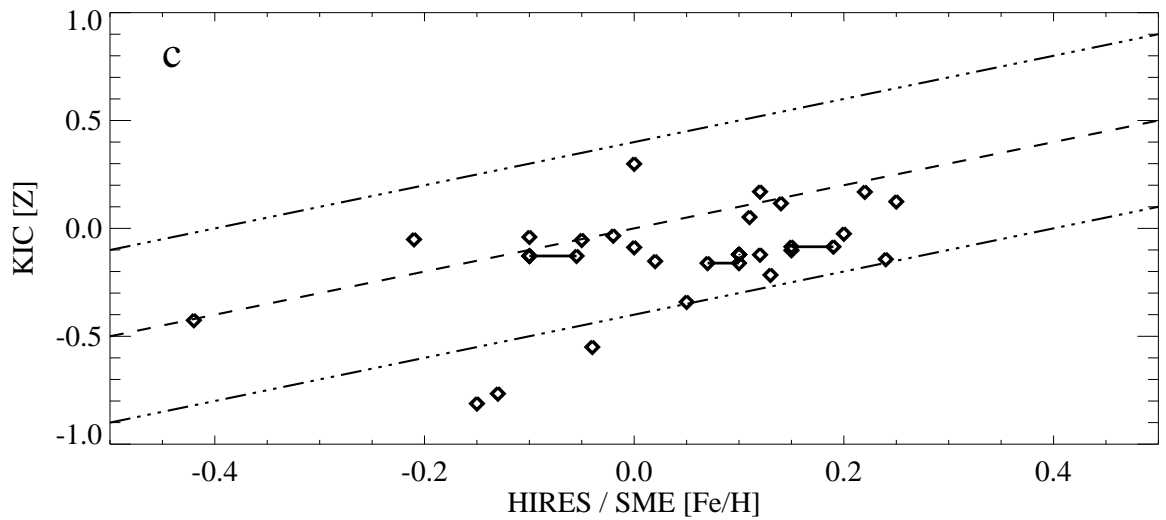
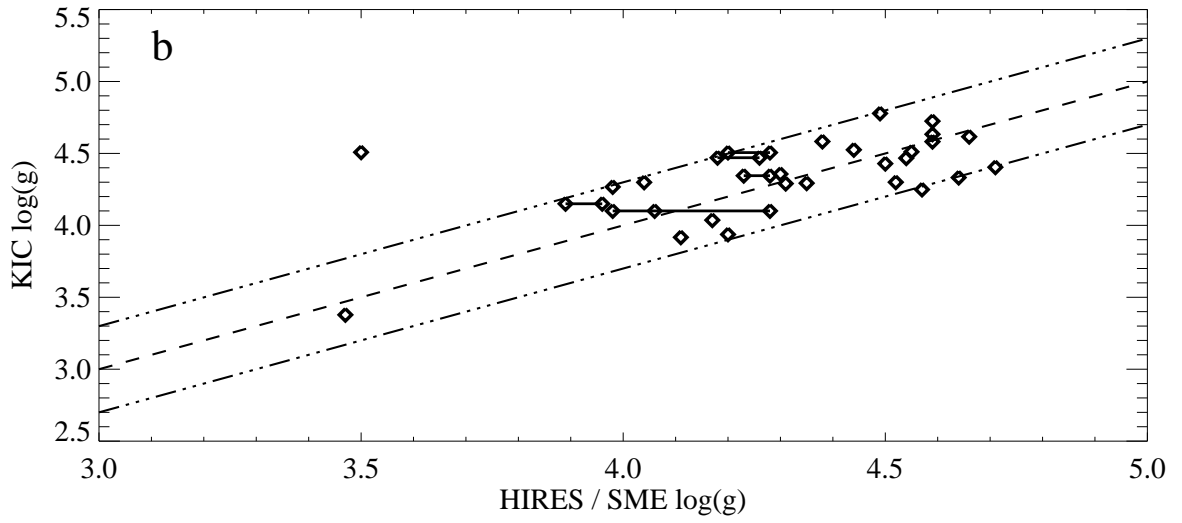
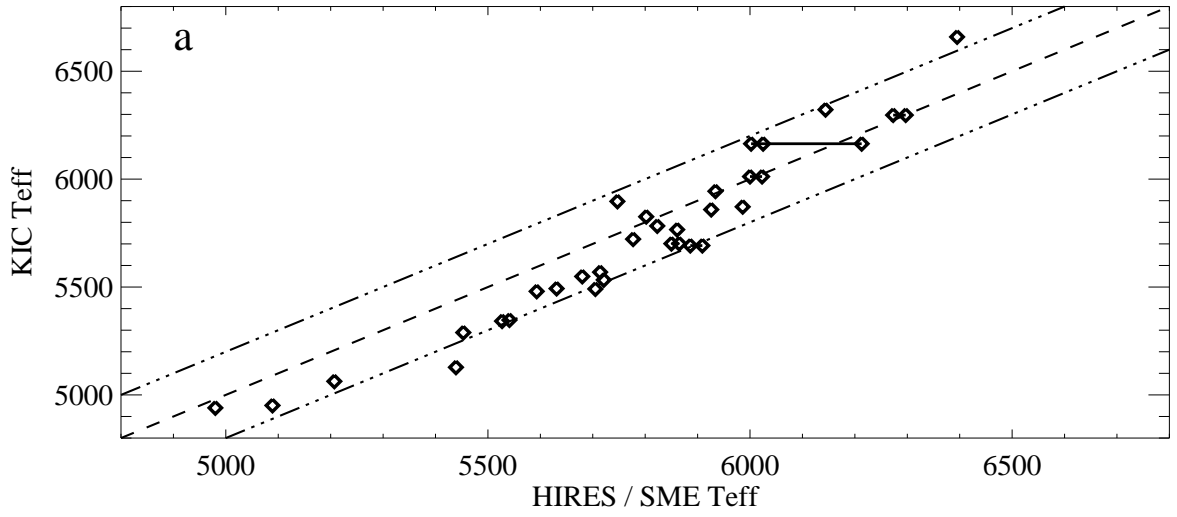


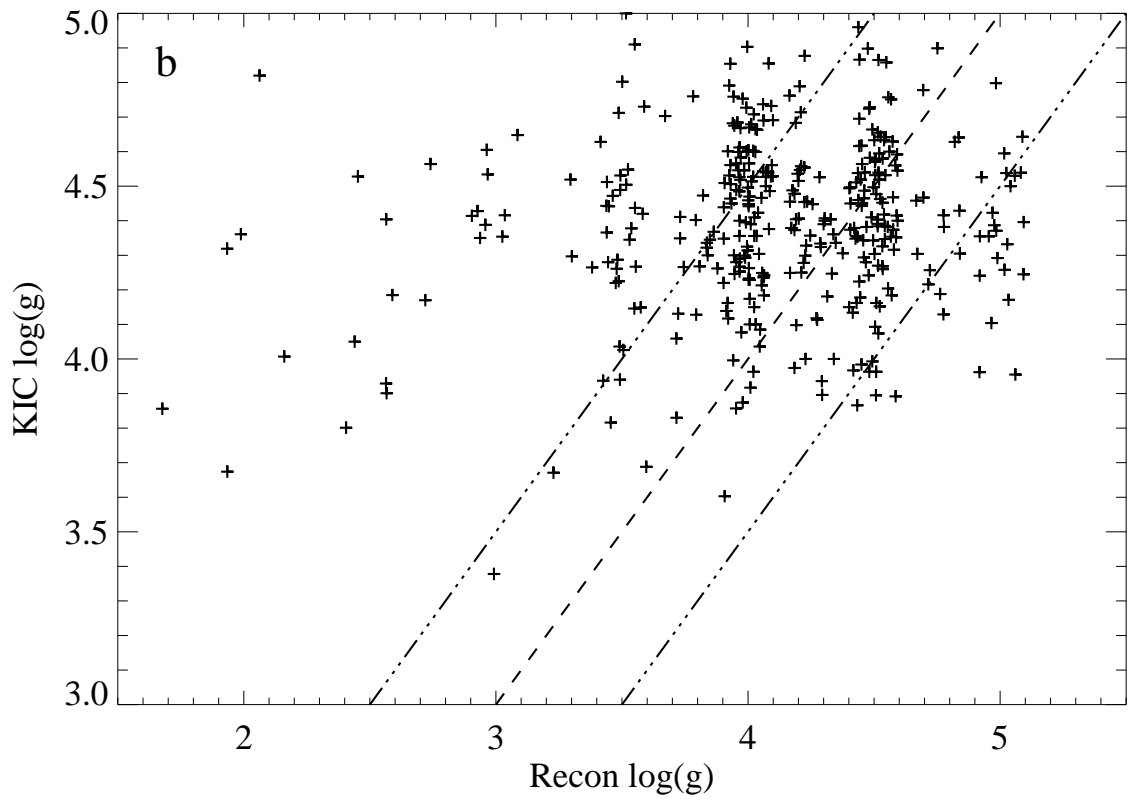
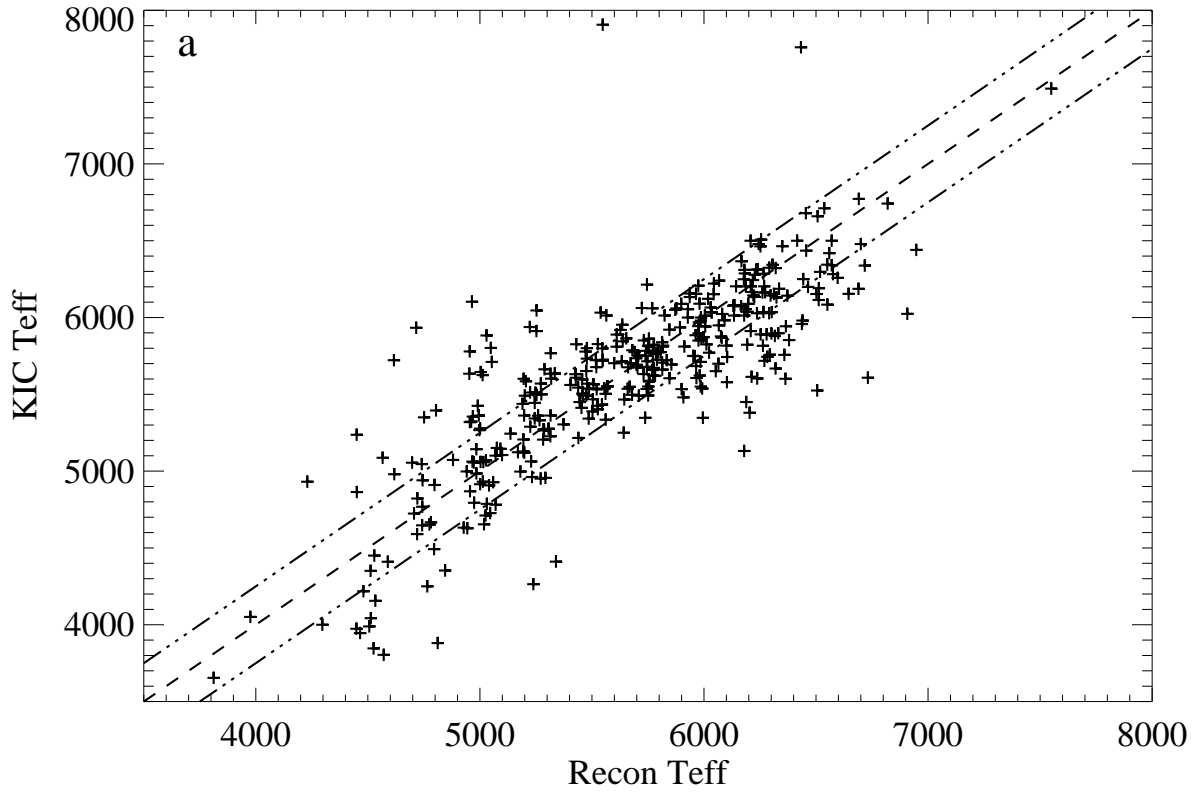


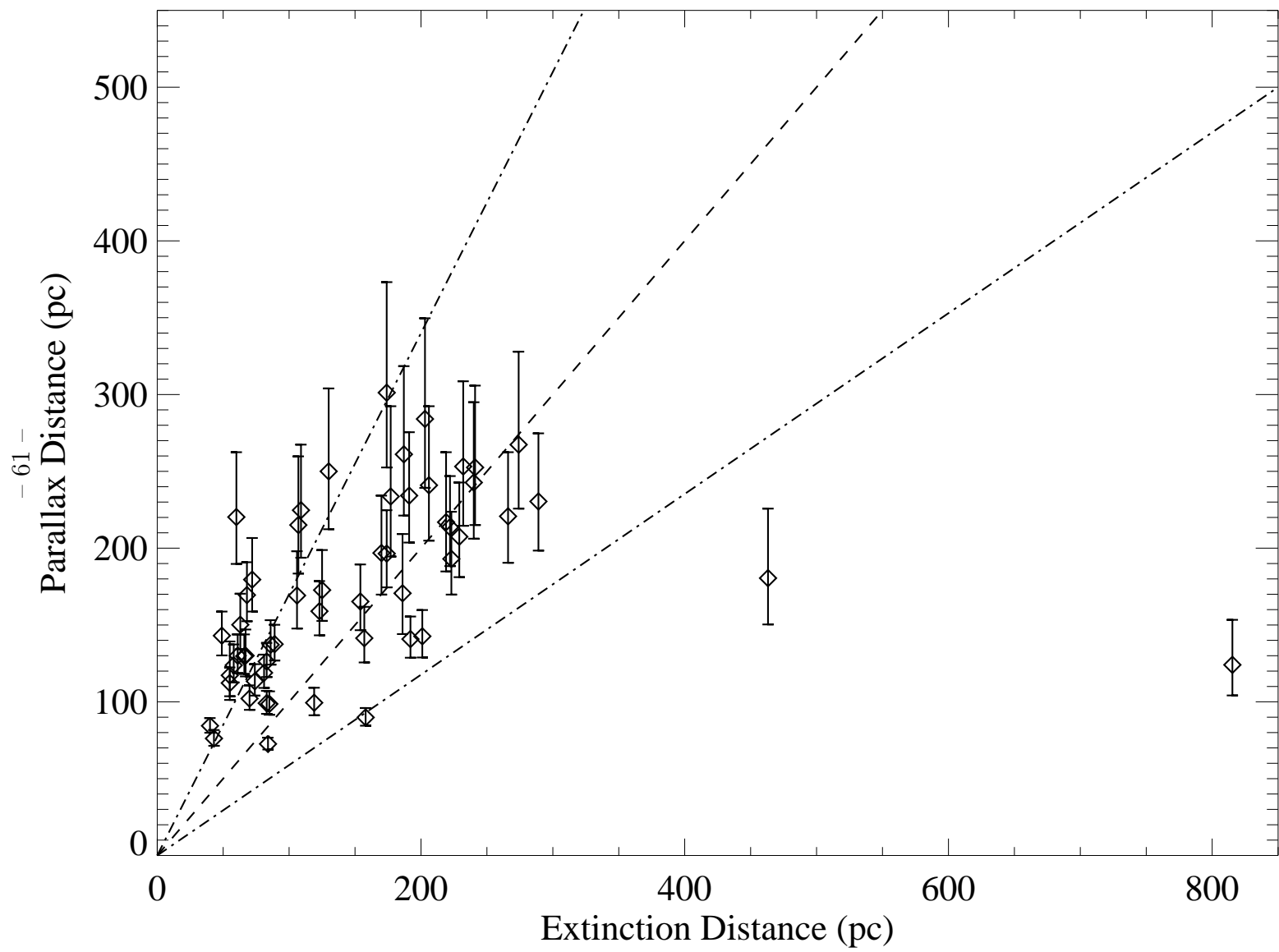


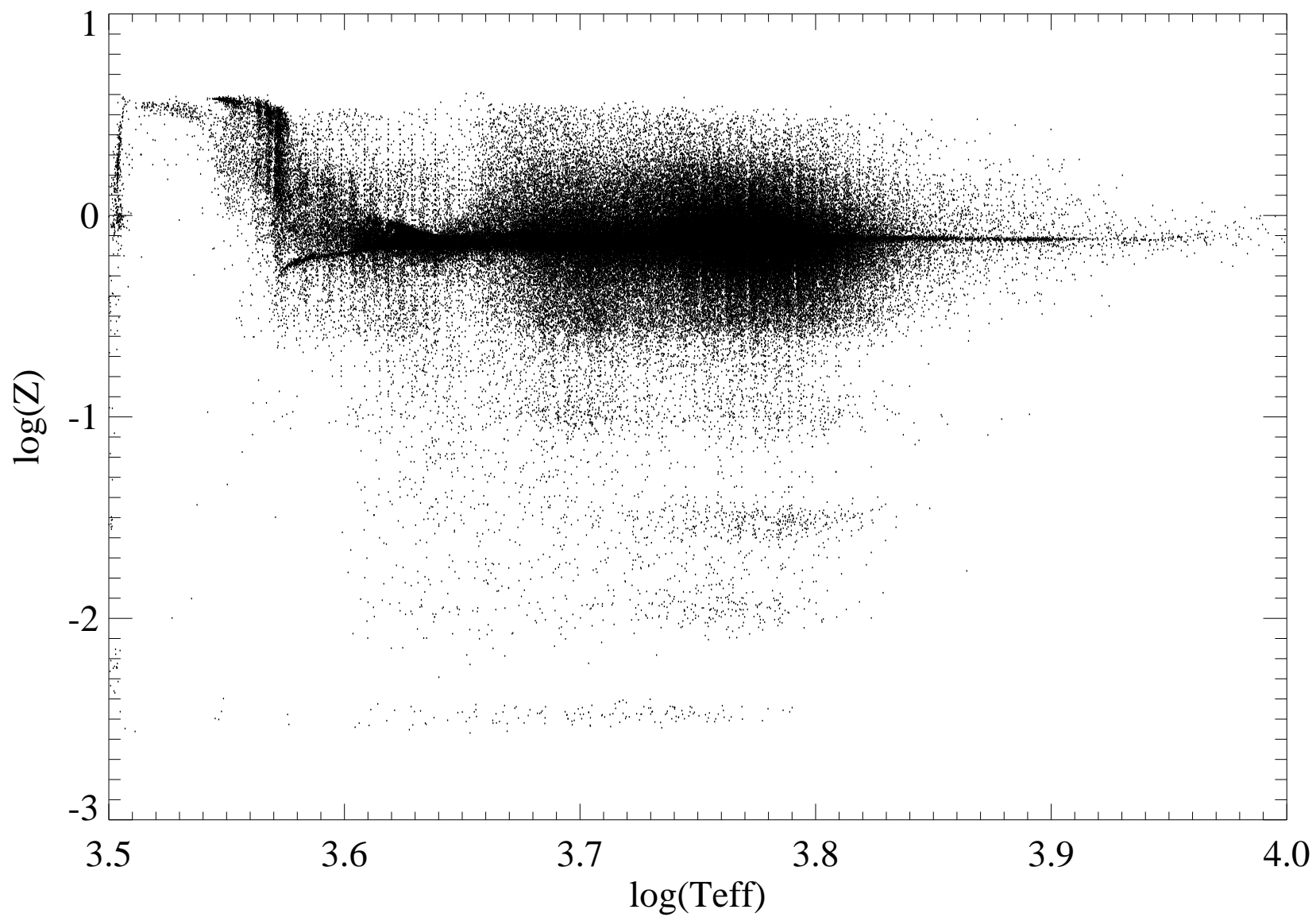












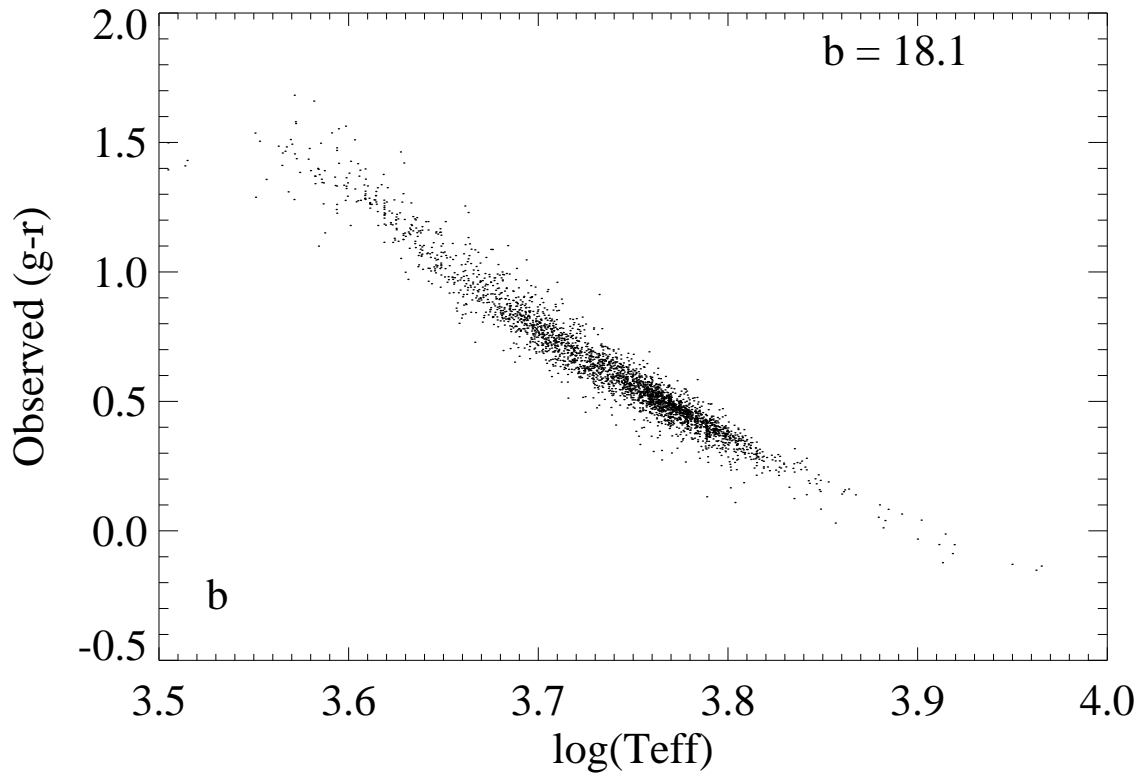
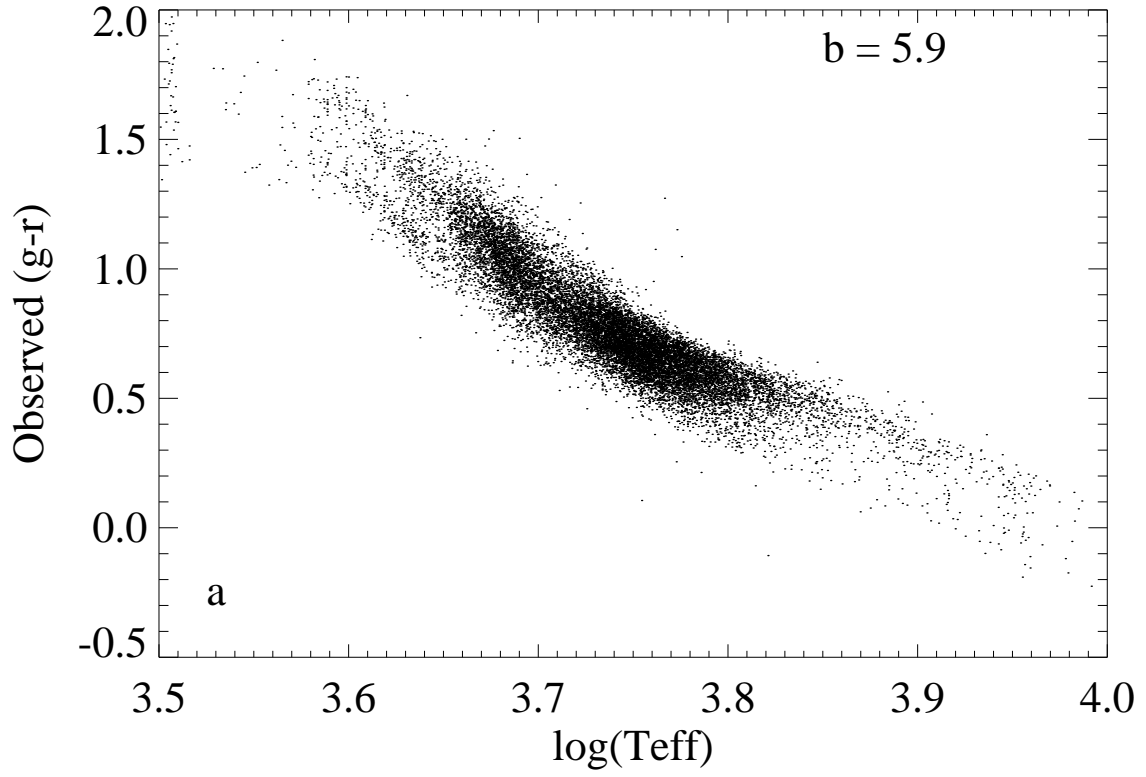


Table 1. KIC primary standard stars.

RA	Dec	u	g	r	i	z	D51	J	H	K	K _p	T _{eff}	log(<i>g</i>)	log(<i>Z</i>)	log(<i>R</i> _*)
112.83372	29.07580	17.829	16.077	15.434	15.226	15.141	15.838	14.221	13.842	13.773	15.481	5386.	4.483	-2.540	-0.021
112.83971	29.02154	16.745	15.344	16.282	14.527	14.407	15.519	13.493	13.037	12.996	16.047	6057.	4.303	-0.187	0.093
112.84009	29.07181	16.619	15.187	14.871	14.405	14.308	15.034	13.361	13.044	12.941	14.640	6023.	4.334	-1.577	0.076
112.85278	29.14279	17.426	16.191	15.712	15.549	15.502	15.995	14.657	14.362	14.285	15.742	6026.	4.441	-1.955	0.019
112.86972	28.85981	17.497	16.380	16.038	15.898	15.861	16.220	15.039	14.877	14.701	16.043	6257.	4.404	-1.608	0.043
112.87161	29.14310	18.962	17.127	16.438	16.205	16.144	16.876	15.185	14.740	14.739	16.482	5234.	4.539	-2.502	-0.057
112.87298	28.92986	18.938	16.629	15.625	15.245	15.023	16.296	13.951	13.371	13.272	15.660	4614.	4.583	-1.682	-0.129
112.87424	29.00252	17.530	16.366	15.968	15.828	15.772	16.191	15.005	14.787	14.676	15.990	6201.	4.427	-1.835	0.030
112.88787	29.02796	17.541	15.929	15.306	15.030	14.932	15.696	13.989	13.586	13.525	15.300	5559.	4.426	-2.504	0.017
112.88976	28.88614	17.904	16.576	16.065	15.903	15.816	16.372	14.951	14.608	14.494	16.105	5988.	4.451	-1.995	0.013

Table 1. KIC primary standard stars.

RA	Dec	u	g	r	i	z	D51	J	H	K	K _p	T _{eff}	log(<i>g</i>)	log(<i>Z</i>)	log(<i>R</i> _*)
112.83372	29.07580	17.829	16.077	15.434	15.226	15.141	15.838	14.221	13.842	13.773	15.481	5386.	4.483	-2.540	-0.021
112.83971	29.02154	16.745	15.344	16.282	14.527	14.407	15.519	13.493	13.037	12.996	16.047	6057.	4.303	-0.187	0.093
112.84009	29.07181	16.619	15.187	14.871	14.405	14.308	15.034	13.361	13.044	12.941	14.640	6023.	4.334	-1.577	0.076
112.85278	29.14279	17.426	16.191	15.712	15.549	15.502	15.995	14.657	14.362	14.285	15.742	6026.	4.441	-1.955	0.019
112.86972	28.85981	17.497	16.380	16.038	15.898	15.861	16.220	15.039	14.877	14.701	16.043	6257.	4.404	-1.608	0.043
112.87161	29.14310	18.962	17.127	16.438	16.205	16.144	16.876	15.185	14.740	14.739	16.482	5234.	4.539	-2.502	-0.057
112.87298	28.92986	18.938	16.629	15.625	15.245	15.023	16.296	13.951	13.371	13.272	15.660	4614.	4.583	-1.682	-0.129
112.87424	29.00252	17.530	16.366	15.968	15.828	15.772	16.191	15.005	14.787	14.676	15.990	6201.	4.427	-1.835	0.030
112.88787	29.02796	17.541	15.929	15.306	15.030	14.932	15.696	13.989	13.586	13.525	15.300	5559.	4.426	-2.504	0.017
112.88976	28.88614	17.904	16.576	16.065	15.903	15.816	16.372	14.951	14.608	14.494	16.105	5988.	4.451	-1.995	0.013
112.89115	29.14516	16.554	15.405	15.000	14.837	14.835	15.229	14.005	13.685	13.647	15.008	6128.	4.434	-1.872	0.025
112.90254	29.10084	17.774	16.360	15.881	15.725	15.631	16.164	14.842	14.428	14.349	15.916	5982.	4.484	-2.480	-0.005
112.90882	28.92956	17.340	15.968	15.445	15.235	15.177	15.761	14.236	13.926	13.837	15.455	5956.	4.450	-2.054	0.013
112.91368	29.06618	17.242	15.691	15.086	14.845	14.758	15.462	13.794	13.394	13.255	15.099	5635.	4.423	-2.495	0.021
112.91662	29.04206	16.983	15.624	15.130	14.929	14.882	15.424	14.015	13.691	13.644	15.138	5962.	4.469	-2.464	0.003
112.91956	28.90477	18.292	16.838	16.316	16.126	16.036	16.631	15.146	14.810	14.784	16.340	5883.	4.473	-2.486	-0.001
112.92464	28.85696	17.635	16.291	15.843	15.701	15.679	16.103	14.898	14.586	14.509	15.878	6051.	4.476	-2.453	0.001
112.92799	29.09224	18.695	16.716	15.879	15.560	15.361	16.427	14.348	13.784	13.707	15.907	4966.	4.524	-2.516	-0.063
112.92924	28.85333	17.135	15.976	15.592	15.454	15.431	15.805	14.608	14.372	14.292	15.611	6200.	4.430	-1.842	0.028
112.93516	28.95189	18.172	16.686	16.117	15.915	15.845	16.467	14.996	14.522	14.532	16.146	5800.	4.464	-2.478	0.002
112.94336	29.06900	18.333	16.921	16.344	16.119	16.007	16.700	15.128	14.657	14.601	16.360	5855.	4.449	-2.039	0.011
112.94620	29.11882	18.432	16.956	16.411	16.198	16.092	16.743	15.172	14.903	14.710	16.426	5797.	4.470	-2.490	-0.001
112.95280	28.96712	18.737	16.680	15.798	15.442	15.298	16.379	14.271	13.675	13.570	15.814	4884.	4.530	-2.489	-0.073
112.96712	29.13251	18.221	16.830	16.322	16.154	16.085	16.627	15.224	14.923	14.856	16.357	5946.	4.471	-2.457	0.002

Table 1—Continued

RA	Dec	u	g	r	i	z	D51	J	H	K	K _p	T _{eff}	log(<i>g</i>)	log(<i>Z</i>)	log(<i>R</i> _*)
112.97078	28.97373	16.805	15.376	15.277	14.517	14.433	15.280	13.460	13.026	12.897	15.302	6258.	4.263	-0.328	0.118
112.97106	29.15487	17.659	16.487	16.034	15.965	15.820	16.298	14.967	14.624	14.496	16.122	6121.	4.424	-1.835	0.030
112.98400	28.92606	16.938	15.424	14.929	14.750	14.713	15.224	13.849	13.570	13.474	14.952	5883.	4.500	-2.513	-0.015
112.98636	29.05146	18.034	16.425	15.780	15.517	15.401	16.186	14.478	14.038	13.875	15.790	5538.	4.457	-2.496	-0.001
112.99858	29.09735	17.741	16.240	15.719	15.567	15.483	16.033	14.637	14.295	14.132	15.769	5858.	4.488	-2.501	-0.009
113.00002	29.15954	17.136	15.888	15.488	15.358	15.321	15.713	14.538	14.285	14.182	15.517	6182.	4.460	-1.966	0.012
113.00294	29.06850	17.992	16.442	15.894	15.682	15.582	16.228	14.717	14.336	14.182	15.910	5748.	4.476	-2.517	-0.005
113.01177	28.88505	17.601	16.033	15.367	15.114	14.993	15.788	14.023	13.582	13.519	15.390	5473.	4.448	-2.470	0.002
113.01623	29.01028	17.664	16.278	15.830	15.663	15.646	16.090	14.840	14.503	14.529	15.848	6052.	4.486	-2.474	-0.004
113.01743	29.05484	17.066	15.435	14.881	14.689	14.609	15.220	13.787	13.477	13.349	14.913	5663.	4.477	-2.505	-0.008
113.02841	28.93859	17.802	16.386	15.894	15.689	15.670	16.187	14.769	14.500	14.473	15.898	5959.	4.472	-2.475	0.001
113.03005	28.97486	17.497	16.353	15.990	15.821	15.827	16.188	15.044	14.717	14.747	15.981	6230.	4.418	-1.756	0.035
113.03155	28.88633	17.907	16.569	16.071	15.924	15.885	16.368	14.974	14.601	14.788	16.118	5975.	4.452	-1.982	0.012
113.03795	29.08655	17.748	16.655	16.281	16.172	16.104	16.487	15.326	15.022	14.877	16.317	6225.	4.400	-1.555	0.044
113.03827	28.89150	18.404	16.872	16.209	15.981	15.847	16.628	14.974	14.506	14.428	16.248	5564.	4.456	-1.992	0.001
113.04273	28.83938	18.293	16.865	16.305	16.109	16.003	16.648	15.026	14.795	14.695	16.336	5735.	4.462	-2.463	0.002
113.04350	28.85695	17.860	16.699	16.295	16.161	16.131	16.523	15.323	15.028	15.092	16.322	6169.	4.427	-1.796	0.029
113.04398	29.03932	17.375	16.225	15.898	15.756	15.756	16.069	14.871	14.689	14.596	15.897	6257.	4.414	-1.750	0.038
113.04411	28.98423	18.158	16.424	15.712	15.409	15.315	16.167	14.317	13.842	13.734	15.714	5332.	4.461	-2.508	-0.011
113.04429	28.97121	17.485	16.361	15.973	15.809	15.808	16.189	15.005	14.635	14.618	15.975	6213.	4.407	-1.620	0.041
113.05009	29.09244	18.118	16.429	15.743	15.470	15.315	16.179	14.345	13.855	13.762	15.758	5396.	4.459	-2.514	-0.007
113.05294	29.09165	18.047	16.704	16.175	15.999	15.905	16.495	15.042	14.755	14.782	16.211	5976.	4.452	-1.997	0.012
113.05674	29.11622	18.058	16.308	15.586	15.314	15.154	16.049	14.131	13.666	13.589	15.612	5285.	4.466	-2.517	-0.015
113.07095	28.87744	19.319	16.780	15.667	15.240	14.992	16.418	13.858	13.330	13.144	15.702	4252.	4.575	-1.793	-0.169

Table 1—Continued

RA	Dec	u	g	r	i	z	D51	J	H	K	K _p	T _{eff}	log(<i>g</i>)	log(<i>Z</i>)	log(<i>R</i> _*)
113.07125	29.11798	17.654	16.482	16.116	15.996	15.967	16.316	15.204	15.021	14.955	16.142	6228.	4.431	-1.870	0.028
113.08269	28.94757	16.913	15.407	14.846	14.645	14.570	15.190	13.650	13.319	13.281	14.874	5685.	4.451	-2.490	0.007
113.08373	29.02580	18.244	16.753	16.185	15.920	15.831	16.534	14.877	14.573	14.403	16.170	5739.	4.460	-2.491	0.003
113.08819	28.84499	18.089	16.495	15.913	15.718	15.619	16.272	14.737	14.330	14.234	15.951	5591.	4.476	-2.508	-0.009
113.08838	29.05024	18.531	16.713	16.011	15.747	15.626	16.459	14.683	14.323	14.185	16.037	5259.	4.509	-2.533	-0.040
113.10443	28.85820	18.541	16.706	15.952	15.702	15.557	16.438	14.580	14.162	14.127	16.003	5123.	4.530	-2.513	-0.057
113.10693	29.06049	17.281	15.631	15.022	14.784	14.717	15.401	13.387	13.086	12.897	15.038	5927.	4.324	-0.452	0.079
113.10693	29.02066	17.531	16.271	15.847	15.687	15.685	16.090	14.788	14.605	14.400	15.862	6146.	4.454	-1.972	0.014
113.11999	28.99631	17.918	16.641	16.163	15.986	15.941	16.446	15.034	14.663	14.589	16.183	6048.	4.450	-1.987	0.015
113.12162	28.86294	16.788	15.555	15.608	15.719	15.813	15.499	15.247	15.180	15.106	15.595	10857.	4.038	-0.128	0.396
113.12440	29.16117	17.562	15.705	14.972	14.679	14.552	15.443	13.544	13.141	12.935	14.987	5110.	4.475	-2.528	-0.027
113.12466	29.13588	17.994	16.749	16.241	16.041	15.996	16.546	15.160	14.887	14.765	16.254	6027.	4.439	-1.942	0.020
113.12849	28.84345	17.843	16.513	16.025	15.886	15.826	16.315	14.983	14.673	14.615	16.074	5995.	4.457	-1.998	0.010
113.12995	29.07486	17.151	15.916	15.491	15.304	15.295	15.735	14.538	14.237	14.102	15.488	6148.	4.449	-1.945	0.017
113.13519	28.84135	16.420	15.195	14.770	14.655	14.601	15.014	13.797	13.512	13.419	14.817	6095.	4.459	-1.964	0.011
113.13669	29.11497	17.489	16.223	15.768	15.590	15.593	16.034	14.766	14.634	14.377	15.780	6100.	4.450	-1.966	0.016
113.13838	29.13793	19.101	17.146	16.273	16.049	15.915	16.847	14.977	14.525	14.271	16.378	5415.	4.467	-0.317	-0.011
113.14059	29.00837	18.009	16.756	16.343	16.167	16.146	16.578	15.336	14.957	15.169	16.344	6148.	4.450	-1.962	0.017
113.14390	29.00225	18.389	16.504	15.737	15.422	15.273	16.233	14.275	13.768	13.635	15.747	5104.	4.503	-2.526	-0.043
113.14396	28.86844	17.761	15.729	14.951	14.680	14.559	15.455	13.576	13.086	12.997	14.995	4923.	4.525	-2.541	-0.067
113.14717	28.94849	17.186	15.609	14.979	14.767	14.646	15.374	13.712	13.321	13.182	15.020	5605.	4.442	-2.502	0.010
113.14981	28.97701	18.478	16.793	16.163	15.895	15.812	16.558	14.893	14.503	14.396	16.164	5473.	4.474	-2.526	-0.012
113.15199	29.12421	17.650	16.230	15.685	15.467	15.445	16.017	14.583	14.294	14.134	15.696	5925.	4.457	-2.030	0.009
113.15269	29.05283	18.512	17.010	16.454	16.253	16.178	16.794	15.260	14.807	14.810	16.480	5768.	4.475	-2.496	-0.004

Table 1—Continued

RA	Dec	u	g	r	i	z	D51	J	H	K	K _p	T _{eff}	log(<i>g</i>)	log(<i>Z</i>)	log(<i>R</i> _*)
113.15297	29.11531	18.826	16.909	16.099	15.752	15.664	16.627	14.673	14.178	14.019	16.099	5045.	4.538	-2.519	-0.065
113.15983	29.14200	17.086	15.810	15.431	15.286	15.301	15.641	14.506	14.269	14.282	15.443	6198.	4.463	-1.965	0.010
113.16072	29.09034	17.617	16.300	15.808	15.598	15.542	16.101	14.641	14.298	14.226	15.809	6016.	4.455	-2.021	0.011
113.16149	28.89940	17.712	16.507	16.081	15.934	15.899	16.325	15.141	14.717	14.746	16.106	6105.	4.438	-1.933	0.022
113.16203	29.00572	18.841	16.775	15.922	15.604	15.467	16.481	14.445	13.856	13.762	15.955	4878.	4.543	-2.507	-0.081
113.16243	29.12796	17.392	16.157	15.692	15.488	15.478	15.965	14.666	14.317	14.230	15.689	6026.	4.434	-1.946	0.023
191.28435	-0.32358	17.264	16.189	15.793	15.645	15.637	16.015	14.746	14.423	14.509	15.808	6048.	4.474	-1.926	0.002
191.28466	-0.42977	19.028	16.366	14.928	14.232	13.894	15.919	12.679	12.035	11.848	14.872	1807.	4.553	-0.250	0.205
191.32330	-0.28643	18.989	16.667	15.732	15.425	15.268	16.352	14.051	13.419	13.311	15.798	4915.	4.597	-0.420	-0.109
191.33378	-0.37664	18.223	16.968	16.497	16.346	16.297	16.775	15.371	15.223	14.852	16.533	5947.	4.525	-2.025	-0.027
191.33479	-0.36946	18.129	16.016	15.180	14.897	14.769	15.727	13.820	13.271	13.156	15.233	4846.	4.588	-2.364	-0.110
191.34010	-0.41548	17.301	15.813	15.221	14.994	14.852	15.588	13.977	13.512	13.448	15.240	5569.	4.480	-2.500	-0.012
191.34167	-0.38789	16.921	15.442	14.916	14.743	14.648	15.234	13.807	13.426	13.320	14.953	5701.	4.473	-2.517	-0.004
191.34808	-0.23305	18.070	16.819	16.341	16.180	16.095	16.624	15.169	14.823	14.651	16.372	5919.	4.515	-2.021	-0.022
191.35760	-0.24623	17.895	16.011	15.298	15.061	14.901	15.754	13.891	13.369	13.430	15.346	5090.	4.547	-2.470	-0.068
191.36189	-0.35801	18.092	16.750	16.223	16.072	15.977	16.542	15.009	14.775	14.528	16.276	5772.	4.515	-2.463	-0.025
191.36218	-0.42707	17.456	16.527	16.182	16.050	16.033	16.367	15.218	14.935	14.768	16.193	6131.	4.482	-1.561	-0.001
191.36576	-0.20754	17.552	16.320	15.876	15.683	15.665	16.134	14.801	14.471	14.358	15.874	5937.	4.490	-1.999	-0.009
191.38720	-0.27579	17.270	16.073	15.599	15.463	15.367	15.879	14.478	14.115	14.076	15.646	5961.	4.475	-1.993	-0.001
191.40710	-0.34321	18.206	16.883	16.370	16.182	16.078	16.679	15.185	14.734	14.782	16.393	5785.	4.520	-2.473	-0.028
191.42898	-0.32475	17.939	16.362	15.762	15.553	15.444	16.135	14.496	14.083	13.887	15.796	5496.	4.510	-2.521	-0.031
191.45712	-0.45848	19.171	17.031	16.148	15.819	15.644	16.730	14.609	14.006	13.907	16.183	4760.	4.611	-2.472	-0.131
191.46855	-0.18927	19.177	16.572	15.214	13.921	13.197	16.146	11.881	11.310	11.111	14.716	3601.	4.503	0.512	-0.204
191.47046	-0.41512	18.490	16.822	16.207	15.947	15.855	16.591	14.981	14.493	14.563	16.210	5388.	4.554	-2.538	-0.059

Table 1—Continued

RA	Dec	u	g	r	i	z	D51	J	H	K	K _p	T _{eff}	log(<i>g</i>)	log(<i>Z</i>)	log(<i>R</i> _*)
191.48135	-0.21765	16.324	15.194	14.680	14.499	14.449	14.989	13.573	13.221	13.105	14.708	5938.	4.428	-1.928	0.024
191.49281	-0.27563	18.592	16.798	16.122	15.895	15.743	16.551	14.869	14.339	14.176	16.166	5232.	4.577	-2.534	-0.078
191.51301	-0.14601	19.412	16.781	15.407	14.740	14.390	16.351	13.173	12.548	12.403	15.352	1807.	4.553	-0.425	0.205
191.53162	-0.31702	19.136	16.460	15.170	14.598	14.217	16.052	13.015	12.425	12.224	15.157	1807.	4.553	-0.500	0.205
191.53368	-0.29048	19.418	16.837	15.685	15.261	14.980	16.465	13.839	13.195	13.064	15.734	4281.	4.571	-1.450	-0.162
191.53389	-0.15238	16.863	15.768	15.404	15.270	15.254	15.603	14.426	14.073	14.028	15.419	6073.	4.460	-1.943	0.010
191.54521	-0.43657	18.236	16.790	16.295	16.102	16.020	16.590	15.205	14.865	14.519	16.308	5780.	4.530	-2.512	-0.034
191.55176	-0.44512	17.722	16.268	15.678	15.457	15.366	16.044	14.471	13.980	13.912	15.700	5672.	4.496	-2.487	-0.017
191.55671	-0.15303	18.515	16.664	15.933	15.651	15.519	16.403	14.474	14.000	13.968	15.955	5068.	4.581	-2.520	-0.088
191.59628	-0.30239	18.484	16.916	16.310	16.121	16.015	16.687	15.131	14.641	14.608	16.360	5542.	4.545	-2.509	-0.048
191.59737	-0.15245	16.633	15.281	14.810	14.672	14.652	15.088	13.756	13.452	13.417	14.855	5855.	4.458	-2.478	0.007
217.55251	-0.07677	17.353	15.959	15.337	15.078	14.969	15.726	14.015	13.451	13.477	15.342	5652.	4.452	-1.950	0.006
217.55504	0.15115	16.484	15.259	15.233	15.253	15.296	15.182	14.676	14.455	14.417	15.240	6616.	4.381	-1.479	0.062
217.55651	-0.01439	17.726	16.444	15.981	15.815	15.760	16.253	14.949	14.496	14.525	16.004	5952.	4.489	-2.051	-0.008
217.57033	-0.11068	16.758	15.261	14.728	14.544	14.533	15.052	13.676	13.271	13.224	14.759	5700.	4.451	-2.483	0.007
217.57090	-0.08564	18.513	17.023	16.463	16.271	16.213	16.806	15.255	14.992	14.740	16.497	5629.	4.529	-2.500	-0.036
217.57291	0.07969	17.984	16.929	16.456	16.224	16.121	16.735	15.300	14.775	14.845	16.436	5962.	4.487	-1.619	-0.007
217.57580	0.19346	16.333	15.224	14.843	14.709	14.666	15.054	13.944	13.544	13.455	14.864	6088.	4.427	-1.912	0.028
217.57940	0.09199	18.631	16.704	15.981	15.690	15.519	16.445	14.553	14.000	13.814	15.994	5033.	4.582	-2.525	-0.090
217.61813	0.02767	17.770	16.478	16.054	15.877	15.821	16.297	14.964	14.618	14.471	16.057	5920.	4.492	-2.470	-0.010
217.63199	-0.10762	19.010	16.630	15.637	15.265	15.088	16.300	13.997	13.387	13.287	15.674	4807.	4.594	-0.467	-0.117
217.63552	0.01020	18.210	16.924	16.448	16.254	16.187	16.730	15.330	14.987	15.939	16.455	5889.	4.499	-1.969	-0.014
217.65411	0.08967	19.067	17.170	16.411	16.126	16.022	16.901	14.981	14.458	14.784	16.439	5057.	4.601	-2.465	-0.100
217.65431	0.15701	16.723	15.507	15.064	14.912	14.879	15.321	14.012	13.712	13.625	15.091	5988.	4.449	-2.004	0.014

Table 1—Continued

RA	Dec	u	g	r	i	z	D51	J	H	K	K _p	T _{eff}	log(<i>g</i>)	log(<i>Z</i>)	log(<i>R</i> _*)
217.65622	0.15278	18.660	16.381	15.373	15.018	14.837	16.047	13.740	13.135	13.016	15.427	4882.	4.584	-0.444	-0.104
217.65721	-0.02410	18.208	15.920	14.957	14.585	14.357	15.598	13.291	12.701	12.542	14.985	4650.	4.580	-1.629	-0.124
217.66397	0.18130	16.669	15.416	14.972	14.828	14.775	15.230	13.881	13.599	13.553	15.005	5970.	4.448	-2.042	0.014
217.67336	-0.11178	16.722	15.140	14.569	14.350	14.248	14.921	13.307	12.898	12.817	14.587	5484.	4.433	-2.530	0.010
217.67943	0.18160	17.238	15.947	15.511	15.351	15.267	15.763	14.367	14.022	13.913	15.530	5934.	4.465	-2.070	0.005
217.68147	0.09814	16.997	15.787	15.334	15.173	15.140	15.599	14.313	13.926	13.891	15.357	5983.	4.456	-1.987	0.010
217.68305	-0.03143	19.414	16.961	15.998	15.666	15.392	16.639	14.311	13.714	13.528	16.054	4572.	4.615	-1.227	-0.152
217.68949	0.03547	18.078	16.714	16.140	15.885	15.771	16.494	14.807	14.182	14.353	16.134	5694.	4.485	-1.952	-0.011
217.69175	0.03768	17.428	16.184	15.730	15.548	15.473	15.995	14.551	14.236	14.167	15.739	5928.	4.468	-2.010	0.003
217.69668	-0.06101	18.032	16.824	16.415	16.301	16.160	16.647	15.423	14.923	14.817	16.458	6000.	4.499	-1.983	-0.012
217.70658	0.11234	16.946	15.776	15.370	15.218	15.183	15.600	14.292	13.960	13.932	15.386	6015.	4.452	-1.976	0.013
217.73060	0.18246	17.723	16.464	16.038	15.885	15.824	16.283	14.871	14.563	14.310	16.059	5960.	4.481	-2.013	-0.003
217.73633	-0.01134	16.899	15.358	14.767	14.534	14.431	15.133	13.537	13.162	13.053	14.781	5581.	4.467	-2.515	-0.004
217.73657	-0.06573	18.920	17.144	16.409	16.127	15.986	16.882	14.980	14.577	14.451	16.432	5173.	4.594	-2.529	-0.091
217.74565	0.15107	18.000	15.766	14.802	14.414	14.207	15.444	13.025	12.467	12.342	14.820	4943.	4.562	-0.461	-0.086
217.74735	0.04833	16.976	15.197	14.607	14.417	14.336	14.973	13.387	13.076	12.935	14.651	5327.	4.486	-2.526	-0.024
217.74783	-0.06499	16.968	15.669	15.203	15.031	14.966	15.477	14.127	13.702	13.669	15.222	5939.	4.470	-2.463	0.002
217.75821	0.03477	17.852	16.746	16.419	16.286	16.229	16.591	15.384	15.071	14.810	16.424	6105.	4.497	-1.952	-0.010
217.76536	-0.08737	18.284	16.840	16.318	16.123	16.075	16.633	15.237	14.816	14.808	16.338	5760.	4.521	-2.506	-0.029
217.76803	0.03491	18.892	16.819	15.975	15.653	15.430	16.528	14.365	13.852	13.699	16.003	4834.	4.588	-2.502	-0.111
217.77186	-0.05486	17.156	16.026	15.650	15.519	15.476	15.858	14.711	14.432	14.365	15.671	6119.	4.470	-1.951	0.005
217.77680	-0.04159	17.711	15.924	15.215	14.948	14.825	15.668	13.852	13.349	13.269	15.241	5206.	4.530	-2.528	-0.054
217.77713	-0.05114	16.632	15.229	14.737	14.575	14.526	15.030	13.660	13.359	13.269	14.771	5872.	4.474	-2.507	-0.002
217.77895	0.21259	18.126	16.329	15.690	15.467	15.266	16.092	14.361	13.951	13.852	15.725	5231.	4.556	-2.532	-0.067

Table 1—Continued

RA	Dec	u	g	r	i	z	D51	J	H	K	K _p	T _{eff}	log(<i>g</i>)	log(<i>Z</i>)	log(<i>R</i> _*)
217.77935	0.11677	17.174	15.914	15.433	15.305	15.259	15.718	14.352	14.060	13.996	15.488	5976.	4.466	-2.009	0.005
217.79182	-0.01724	16.876	15.394	14.804	14.553	14.438	15.170	13.523	13.067	12.916	14.805	5603.	4.453	-2.491	0.004
217.79201	0.00951	18.670	17.074	16.440	16.189	16.056	16.838	15.000	14.580	14.420	16.455	5421.	4.544	-2.505	-0.052
217.79742	0.07924	19.249	16.921	15.930	15.571	15.376	16.592	14.394	13.756	13.644	15.976	4937.	4.599	-0.383	-0.108
217.79915	-0.10460	16.980	15.265	14.673	14.473	14.438	15.040	13.519	13.135	13.035	14.711	5407.	4.481	-2.529	-0.018
217.80669	-0.11325	17.558	16.676	16.426	16.298	16.302	16.541	15.522	15.303	14.980	16.489	6166.	4.479	-1.528	0.001
217.82412	-0.06026	18.249	16.452	15.718	15.365	15.214	16.190	14.176	13.595	13.441	15.691	5131.	4.560	-2.507	-0.074
217.83137	-0.09757	16.919	15.662	15.194	15.021	15.034	15.470	14.086	13.727	13.691	15.213	5993.	4.459	-2.010	0.009
217.83537	-0.01802	19.259	17.220	16.454	16.182	16.064	16.950	15.105	14.525	14.646	16.493	4944.	4.619	-2.495	-0.118
217.83774	0.03891	16.862	15.931	15.586	15.440	15.418	15.771	14.619	14.355	14.292	15.587	6165.	4.435	-1.541	0.025
217.85721	0.11197	16.923	15.759	15.329	15.159	15.141	15.577	14.287	14.019	13.926	15.339	6041.	4.456	-1.968	0.011
217.85812	-0.06374	18.303	16.775	16.213	15.995	15.945	16.558	15.003	14.510	14.452	16.229	5572.	4.521	-2.513	-0.034
217.86380	-0.03107	17.377	16.275	15.895	15.739	15.734	16.106	14.935	14.585	14.589	15.900	6072.	4.473	-1.942	0.003
217.86569	0.03627	18.056	16.810	16.304	16.074	16.030	16.608	15.198	14.683	14.865	16.295	5920.	4.493	-1.971	-0.011
237.83842	0.02185	17.374	16.252	16.023	15.939	15.950	16.122	15.153	15.006	15.009	16.081	6290.	4.460	-1.889	0.014
237.84085	-0.02041	17.358	15.981	15.512	15.313	15.245	15.788	14.367	13.989	13.983	15.513	5792.	4.462	-2.489	0.003
237.84333	0.01140	18.048	16.270	15.548	15.239	15.095	16.011	14.102	13.603	13.509	15.548	5137.	4.546	-2.527	-0.066
237.84367	0.10028	16.879	15.525	15.024	14.825	14.760	15.324	13.888	13.615	13.400	15.035	5816.	4.459	-2.469	0.005
237.84485	-0.09163	18.030	16.643	16.141	15.941	15.865	16.441	14.992	14.801	14.516	16.151	5741.	4.484	-2.485	-0.010
237.84861	-0.05889	17.399	15.590	14.878	14.608	14.454	15.333	13.462	12.974	12.913	14.902	5111.	4.508	-2.519	-0.045
237.85056	0.20356	19.059	17.044	16.238	15.918	15.764	16.763	14.757	14.230	14.077	16.256	4852.	4.591	-2.536	-0.111
237.85340	0.16137	18.961	17.070	16.305	15.944	15.791	16.800	14.493	13.848	13.878	16.282	4970.	4.578	-2.471	-0.093
237.85422	0.14113	18.977	16.497	15.505	15.132	14.954	16.167	13.842	13.305	13.172	15.542	4402.	4.585	-2.075	-0.154
237.85493	0.18554	19.566	17.118	16.064	15.648	15.438	16.772	14.330	13.685	13.583	16.089	4327.	4.592	-1.745	-0.169

Table 1—Continued

RA	Dec	u	g	r	i	z	D51	J	H	K	K _p	T _{eff}	log(<i>g</i>)	log(<i>Z</i>)	log(<i>R</i> _*)
237.85646	0.05079	17.419	15.638	14.893	14.594	14.448	15.373	13.512	12.917	12.782	14.907	5128.	4.528	-2.504	-0.056
237.85780	0.01452	17.651	16.414	15.957	15.773	15.707	16.225	14.881	14.518	14.510	15.965	5967.	4.467	-1.993	0.004
237.86071	0.21626	17.246	16.045	15.620	15.439	15.354	15.864	14.448	14.102	14.138	15.621	6023.	4.447	-1.986	0.016
237.88140	-0.11614	18.529	16.400	15.503	15.151	14.976	16.095	13.862	13.294	13.226	15.525	4733.	4.573	-2.353	-0.112
237.88755	0.18246	17.800	16.148	15.541	15.314	15.201	15.919	14.294	13.839	13.785	15.564	5402.	4.513	-2.532	-0.036
237.89129	0.07838	17.433	16.261	15.838	15.655	15.584	16.080	14.702	14.394	14.153	15.837	6012.	4.455	-1.961	0.011
237.89665	0.14853	16.988	15.508	14.963	14.739	14.658	15.296	13.695	13.308	13.256	14.970	5643.	4.458	-2.495	0.002
237.89916	0.16769	16.948	15.454	14.936	14.727	14.658	15.249	13.733	13.385	13.342	14.945	5684.	4.468	-2.511	-0.002
237.90057	0.16001	18.106	16.924	16.495	16.315	16.243	16.742	15.410	14.954	14.721	16.498	5984.	4.482	-1.970	-0.004
237.90277	-0.01556	18.620	16.332	15.401	15.057	14.815	16.018	13.694	13.185	13.057	15.439	4643.	4.585	-1.763	-0.128
237.90829	0.00290	18.089	16.891	16.431	16.239	16.160	16.701	15.269	14.987	15.125	16.435	5948.	4.478	-1.964	-0.002
237.91767	0.17409	16.422	15.103	14.637	14.782	14.373	14.911	13.441	13.109	13.090	14.878	6320.	4.316	-0.369	0.091
237.91935	0.06420	16.740	15.352	14.858	14.665	14.604	15.153	13.675	13.321	13.253	14.871	5801.	4.460	-2.489	0.005
237.92210	0.12322	18.020	16.564	16.020	15.802	15.712	16.352	14.746	14.382	14.223	16.031	5639.	4.492	-2.496	-0.016
237.92253	0.17904	16.289	15.082	14.773	14.653	14.639	14.931	13.782	13.519	13.505	14.782	6198.	4.452	-1.998	0.016
237.93646	0.20180	19.464	16.790	15.369	14.701	14.321	16.348	13.105	12.439	12.243	15.328	1807.	4.553	-0.425	0.205
237.93735	0.17903	17.825	16.491	16.013	15.811	15.748	16.296	14.855	14.448	14.372	16.015	5826.	4.481	-2.474	-0.006
237.94127	0.14902	18.774	16.987	16.348	16.088	15.993	16.750	15.035	14.569	14.583	16.358	5217.	4.569	-2.545	-0.075
237.94943	-0.03663	18.099	16.873	16.410	16.247	16.148	16.681	15.230	14.855	14.907	16.434	5940.	4.476	-1.976	-0.001
237.95215	0.07177	17.619	16.232	15.740	15.584	15.511	16.033	14.608	14.260	14.144	15.779	5842.	4.479	-2.495	-0.005
237.95948	0.14660	17.994	15.867	15.005	14.680	14.507	15.571	13.390	12.882	12.782	15.036	4770.	4.554	-2.475	-0.097
237.96244	0.20353	18.275	16.821	16.242	16.021	15.907	16.600	14.891	14.426	14.353	16.261	5604.	4.493	-2.492	-0.018
237.96250	0.15749	18.341	15.723	14.534	14.335	13.791	15.342	12.592	11.957	11.832	14.752	4620.	4.604	-0.213	-0.141
237.97368	-0.06294	19.336	17.144	16.235	15.899	15.697	16.836	14.619	14.012	13.987	16.272	4670.	4.602	-2.441	-0.135

Table 1—Continued

RA	Dec	u	g	r	i	z	D51	J	H	K	K _p	T _{eff}	log(<i>g</i>)	log(<i>Z</i>)	log(<i>R</i> _*)
237.97832	0.01233	18.017	16.780	16.291	16.106	16.020	16.582	15.127	14.739	14.797	16.308	5931.	4.473	-1.984	-0.000
237.98634	0.17846	17.926	16.624	16.197	16.047	15.989	16.442	15.041	14.787	14.778	16.220	5966.	4.487	-2.470	-0.007
237.99854	0.01422	17.672	16.644	16.253	16.099	16.010	16.472	15.227	14.800	14.789	16.263	6058.	4.455	-1.875	0.012
238.00153	-0.04527	16.248	15.050	14.627	14.466	14.420	14.869	13.564	13.246	13.175	14.641	6015.	4.432	-1.989	0.023
238.00189	0.13213	18.677	17.046	16.393	16.135	16.008	16.805	15.022	14.494	14.352	16.408	5349.	4.541	-2.520	-0.054
238.00876	-0.02231	18.014	16.685	16.171	15.964	15.888	16.480	14.939	14.538	14.457	16.180	5764.	4.479	-2.455	-0.006
238.01165	-0.07760	14.944	15.020	15.402	15.679	15.968	15.050	15.535	15.717	15.657	15.306	6430.	4.288	-0.240	0.108
238.01712	0.03076	16.930	15.668	15.154	14.975	14.894	15.464	13.981	13.643	13.554	15.183	5920.	4.440	-1.993	0.017
238.01786	-0.08414	16.829	15.429	14.926	14.732	14.673	15.227	13.795	13.426	13.416	14.941	5835.	4.459	-2.494	0.006
238.02136	-0.11267	18.617	16.985	16.335	16.051	15.921	16.744	14.958	14.523	14.433	16.331	5388.	4.533	-2.521	-0.048
238.02696	0.00142	18.884	17.149	16.414	16.132	15.973	16.887	14.945	14.393	14.460	16.437	5165.	4.569	-2.515	-0.077
238.03477	-0.01388	17.034	15.562	15.020	14.813	14.755	15.350	13.814	13.496	13.377	15.037	5720.	4.456	-2.501	0.005
238.03592	-0.05534	18.362	16.875	16.275	16.012	15.877	16.648	14.896	14.449	14.317	16.271	5571.	4.498	-2.488	-0.021
238.03833	-0.06382	18.004	16.656	16.140	15.909	15.816	16.451	14.874	14.416	14.615	16.133	5852.	4.471	-2.044	-0.000
238.04117	0.12216	16.767	15.263	14.608	16.006	14.208	15.022	13.189	12.724	12.648	15.783	5875.	4.330	-0.151	0.075
238.04686	0.19165	18.440	16.506	15.556	15.185	14.955	16.187	13.801	13.194	13.073	15.581	4942.	4.561	-1.727	-0.086
238.04853	-0.03701	17.261	15.739	15.208	14.996	14.911	15.530	14.003	13.592	13.496	15.219	5679.	4.463	-2.516	0.000
238.05395	0.16804	17.836	16.554	16.065	15.879	15.802	16.356	14.840	14.522	14.358	16.082	5904.	4.469	-2.013	0.002
238.05678	0.20036	17.376	15.561	14.908	14.698	14.596	15.320	13.618	13.294	13.160	14.957	5239.	4.519	-2.521	-0.046
238.05726	0.16876	18.095	15.866	14.975	14.674	14.527	15.563	13.462	12.977	12.859	15.032	4704.	4.579	-2.335	-0.118
238.05777	0.12956	18.988	17.002	16.214	15.965	15.824	16.726	14.794	14.388	14.414	16.276	4965.	4.592	-2.491	-0.101
238.05882	0.08982	18.381	16.733	16.029	15.765	15.600	16.479	14.592	14.112	14.076	16.056	5292.	4.536	-2.508	-0.053
238.06906	0.15327	17.570	16.150	15.586	15.388	15.300	15.933	14.335	13.935	13.887	15.617	5701.	4.468	-2.474	-0.002
238.07432	0.00539	17.455	15.784	15.164	14.951	14.852	15.552	13.904	13.599	13.519	15.201	5414.	4.494	-2.527	-0.025

Table 1—Continued

RA	Dec	u	g	r	i	z	D51	J	H	K	K _p	T _{eff}	log(<i>g</i>)	log(<i>Z</i>)	log(<i>R</i> _*)
238.07871	0.02938	17.616	16.386	15.914	15.730	15.638	16.193	14.734	14.416	14.272	15.927	5957.	4.462	-2.003	0.007
238.08637	-0.05511	18.050	16.851	16.407	16.252	16.166	16.664	15.307	15.042	14.888	16.431	6018.	4.479	-1.983	-0.001
238.09978	0.20276	17.775	16.074	15.440	15.230	15.142	15.838	14.188	13.794	13.760	15.483	5370.	4.508	-2.530	-0.035
238.10008	-0.06328	16.710	15.358	14.835	14.656	14.575	15.151	13.711	13.342	13.295	14.866	5846.	4.452	-2.471	0.010
238.10388	-0.08774	17.588	16.076	15.410	15.153	14.998	15.831	13.999	13.539	13.398	15.430	5574.	4.454	-2.007	0.002
238.11271	-0.09489	18.824	17.121	16.326	15.989	15.769	16.842	14.757	14.191	13.967	16.328	5147.	4.570	-2.488	-0.079
238.11979	-0.10813	17.642	16.278	15.739	15.554	15.451	16.067	14.555	14.188	14.057	15.771	5799.	4.470	-2.461	-0.001
238.13630	0.15989	17.766	16.426	15.843	15.586	15.426	16.204	14.423	13.980	13.977	15.838	5717.	4.455	-1.982	0.005
238.15377	0.13531	17.370	16.094	15.590	15.417	15.320	15.892	14.425	14.048	13.951	15.620	5895.	4.451	-1.996	0.011
238.15832	0.04735	17.916	16.761	16.287	16.131	16.049	16.567	15.198	14.836	14.701	16.320	5981.	4.466	-1.921	0.005
238.15995	0.02711	18.163	16.728	16.133	15.909	15.773	16.502	14.819	14.429	14.266	16.155	5607.	4.489	-2.474	-0.015
238.16131	0.00685	17.992	16.196	15.505	15.252	15.117	15.945	14.112	13.688	13.480	15.535	5186.	4.529	-2.530	-0.054
238.16132	0.02879	18.975	16.842	16.022	15.752	15.572	16.557	14.519	13.999	13.839	16.079	4815.	4.587	-2.469	-0.113
259.65052	27.14874	17.762	16.104	15.475	15.281	15.178	15.869	14.244	13.916	13.852	15.528	5414.	4.494	-2.506	-0.025
259.65958	26.84594	19.058	16.545	15.439	15.066	14.814	16.185	13.691	13.054	12.939	15.509	4308.	4.582	-1.503	-0.165
259.66374	26.99608	16.942	15.639	15.158	15.012	14.921	15.443	14.086	13.744	13.696	15.200	5908.	4.441	-2.001	0.017
259.67819	27.15510	17.517	16.033	15.472	15.269	15.159	15.816	14.316	13.877	13.855	15.498	5632.	4.461	-2.489	0.000
259.69221	26.86024	17.878	16.257	15.692	15.547	15.469	16.039	14.589	14.262	14.301	15.760	5569.	4.484	-2.493	-0.014
259.69259	26.95007	18.695	17.135	16.450	16.218	16.064	16.885	15.076	14.589	14.608	16.493	5328.	4.536	-2.484	-0.052
259.69812	27.11474	17.659	16.338	15.838	15.649	15.586	16.137	14.734	14.394	14.378	15.856	5827.	4.458	-2.445	0.006
259.70203	27.12271	17.787	16.109	15.435	15.167	15.032	15.862	14.057	13.602	13.580	15.450	5286.	4.496	-2.513	-0.031
259.70280	27.10008	18.613	16.831	16.113	15.829	15.695	16.573	14.715	14.262	14.103	16.130	5153.	4.547	-2.530	-0.065
259.70427	26.84051	19.287	17.264	16.428	16.176	16.008	16.975	14.945	14.528	14.406	16.502	4871.	4.592	-2.485	-0.110
259.72331	26.90277	18.059	16.465	15.845	15.642	15.534	16.233	14.634	14.252	14.297	15.889	5481.	4.498	-2.503	-0.025

Table 1—Continued

RA	Dec	u	g	r	i	z	D51	J	H	K	K _p	T_{eff}	$\log(g)$	$\log(Z)$	$\log(R_*)$
259.73238	27.02563	18.011	16.215	15.534	15.292	15.168	15.966	14.157	13.769	13.577	15.569	5177.	4.525	-2.529	-0.052
259.73472	26.90265	18.404	16.581	15.879	15.625	15.472	16.327	14.535	14.051	13.923	15.912	5159.	4.543	-2.535	-0.063
259.74484	27.03135	17.933	16.652	16.259	16.115	16.088	16.479	15.304	14.928	14.935	16.276	6026.	4.473	-2.451	0.002
259.75119	26.95386	17.175	15.932	15.445	15.274	15.182	15.734	14.400	13.978	13.949	15.471	5919.	4.434	-1.941	0.021
259.76265	27.15650	16.786	15.407	14.911	15.408	14.673	15.207	13.801	13.518	13.410	15.408	6165.	4.279	-0.195	0.108
259.76382	27.08831	17.191	15.967	15.503	15.327	15.259	15.776	14.374	14.050	14.058	15.519	5946.	4.434	-1.957	0.021
259.76990	26.93250	17.888	16.048	15.300	15.015	14.826	15.782	13.823	13.310	13.220	15.325	5046.	4.528	-2.517	-0.059
259.77336	27.09114	18.102	16.896	16.454	16.308	16.252	16.710	15.362	15.138	14.867	16.484	5985.	4.462	-1.955	0.007
259.77711	26.98755	18.031	16.747	16.261	16.092	16.038	16.550	15.122	14.958	14.678	16.289	5884.	4.460	-1.981	0.006
259.78401	27.05101	18.909	16.833	15.995	15.699	15.542	16.544	14.512	13.993	13.903	16.039	4808.	4.577	-2.510	-0.107
259.78411	27.07716	17.147	15.816	15.360	15.226	15.170	15.626	14.324	14.031	13.951	15.403	5952.	4.456	-2.050	0.009
259.78879	27.02063	16.679	15.550	15.161	15.012	14.994	15.378	14.121	13.833	13.743	15.173	6077.	4.419	-1.922	0.031
259.79339	27.12356	18.043	16.549	16.007	15.852	15.763	16.337	14.907	14.570	14.602	16.061	5697.	4.477	-2.478	-0.007
259.79969	27.13828	18.994	17.161	16.445	16.187	16.047	16.903	15.125	14.566	14.538	16.479	5132.	4.568	-2.531	-0.078
259.80008	27.09228	17.856	16.698	16.276	16.118	16.063	16.518	15.285	14.912	14.627	16.292	6019.	4.450	-1.930	0.014
259.80108	27.01536	17.132	15.632	15.099	14.920	14.862	15.422	13.989	13.637	13.544	15.134	5654.	4.465	-2.495	-0.001
259.81278	26.91399	18.228	16.519	15.884	15.645	15.545	16.283	14.660	14.289	14.178	15.907	5347.	4.524	-2.535	-0.044
259.82489	27.10241	17.064	15.946	15.562	15.399	15.344	15.776	14.467	14.178	14.221	15.564	6129.	4.427	-1.894	0.029
259.83651	26.87406	17.990	16.677	16.235	16.076	15.992	16.492	15.167	14.827	14.798	16.257	5950.	4.475	-2.456	-0.000
259.85172	27.13008	17.202	15.326	14.636	14.417	14.313	15.076	13.323	12.951	12.811	14.689	5152.	4.520	-2.562	-0.051
259.85254	26.88590	17.752	16.375	15.885	15.678	15.606	16.177	14.766	14.368	14.298	15.887	5823.	4.468	-2.476	0.001
259.85331	27.14967	19.112	17.211	16.430	16.140	15.968	16.937	14.913	14.355	14.407	16.462	5010.	4.572	-2.523	-0.086
259.85891	26.97853	18.014	16.277	15.577	15.322	15.164	16.023	14.217	13.694	13.643	15.608	5197.	4.525	-2.514	-0.051
259.86462	26.98412	18.013	16.219	15.538	15.295	15.158	15.970	14.204	13.785	13.683	15.572	5185.	4.529	-2.534	-0.054

Table 1—Continued

RA	Dec	u	g	r	i	z	D51	J	H	K	K _p	T_{eff}	$\log(g)$	$\log(Z)$	$\log(R_*)$
259.86484	27.05211	17.055	15.573	15.055	14.830	14.701	15.368	13.769	13.384	13.301	15.053	5659.	4.437	-2.509	0.014
259.86734	27.03491	17.696	16.490	16.043	15.878	15.820	16.303	15.025	14.632	14.542	16.062	5984.	4.449	-1.952	0.014
259.87710	26.92754	19.118	16.993	16.147	15.811	15.615	16.702	14.509	13.996	13.877	16.166	4765.	4.577	-2.505	-0.111
259.88023	27.02556	17.858	16.496	16.054	15.896	15.819	16.311	15.003	14.624	14.923	16.076	5935.	4.472	-2.466	0.001
259.88697	26.89465	17.416	15.971	15.453	15.260	15.172	15.766	14.272	13.922	13.798	15.474	5745.	4.465	-2.500	0.001
259.88724	26.98993	18.128	16.609	16.036	15.835	15.698	16.389	14.861	14.345	14.339	16.067	5595.	4.485	-2.496	-0.013
259.89797	26.89960	17.172	15.830	15.353	15.186	15.113	15.635	14.244	13.949	13.820	15.379	5936.	4.455	-2.060	0.010
259.90723	27.12719	17.176	15.648	15.097	14.887	14.806	15.434	13.849	13.451	13.349	15.116	5681.	4.453	-2.509	0.006
259.91003	26.95877	18.064	16.461	15.844	15.635	15.535	16.230	14.617	14.183	14.057	15.883	5471.	4.496	-2.512	-0.024
259.91250	26.86580	17.207	15.999	15.600	15.461	15.409	15.825	14.593	14.242	14.170	15.623	6087.	4.445	-1.973	0.018
259.91387	27.11470	17.538	16.381	15.960	15.785	15.722	16.201	14.868	14.458	14.396	15.964	6076.	4.443	-1.946	0.019
259.91849	26.96707	17.630	16.075	15.450	15.215	15.077	15.842	14.132	13.685	13.653	15.473	5480.	4.467	-2.504	-0.008
259.92717	26.87529	18.463	16.786	16.167	15.961	15.845	16.554	14.909	14.435	14.406	16.209	5389.	4.518	-2.536	-0.040
259.96336	27.15429	17.538	16.346	16.088	15.986	15.981	16.209	15.196	14.871	15.022	16.153	6283.	4.457	-1.953	0.015
259.96346	26.98795	18.318	16.468	15.724	15.476	15.344	16.203	14.423	13.935	13.861	15.774	5141.	4.544	-2.544	-0.064
259.96610	27.15692	18.778	16.975	16.370	16.150	16.068	16.747	15.101	14.744	14.601	16.398	5325.	4.534	-2.522	-0.051
259.96910	26.90105	17.771	16.090	15.474	15.321	15.210	15.859	14.311	13.948	13.923	15.552	5404.	4.504	-2.499	-0.031
259.97117	26.90373	17.173	15.623	15.014	14.814	14.685	15.394	13.768	13.294	13.269	15.057	5488.	4.455	-2.494	-0.001
259.98064	27.00302	17.828	15.649	14.800	14.495	14.295	15.357	13.239	12.678	12.574	14.841	4732.	4.544	-2.403	-0.094
259.98246	26.99972	17.573	16.199	15.565	15.333	15.177	15.963	14.220	13.784	13.650	15.593	5666.	4.437	-1.948	0.014

